EXPLORING THE SENSORIMOTOR NETWORK USING FUNCTIONAL CONNECTIVITY AND GRAPH THEORY

by

Ronald Bishop

Submitted in partial fulfillment of the requirements for the degree of Master of Science

at

Dalhousie University
Halifax, Nova Scotia
August 2014

TABLE OF CONTENTS

LIST OF TABLES

LIST OF FIGURES

ABSTRACT

Background: Performing a motor task activates the sensorimotor network. Functional connectivity (FC) analysis can determine connections between distinct neural regions of a network. Graph theory can then be applied to quantify the network's connections. Establishing the network in non-disabled participants can be used as a comparator in future neuroimaging research. **Purpose:** To determine the sensorimotor network in a group of non-disabled participants. **Methods:** Nineteen participants were scanned using magnetoencephalography while they performed a unilateral upper-limb visuomotor task. FC was compared between rest and task conditions to determine significant connections during task only. These connections were quantified using graph theory.
Results: FC significantly increased between 118 node pairs during the task state compared to rest. Graph theory quantitatively highlighted 40 nodes as important, including regions of the pre-established sensorimotor network (contralateral primary motor and somatosensory cortex among others). This network can be used as a template for comparison in future studies.

LIST OF ABBREVIATIONS USED

1DI first dorsal interosseous

AG angular gyrus

BEM boundary element model

BOLD blood oxygen level dependent

BSR bootstrap ratio

C clustering coefficient

CB cerebellum

CC cingulate cortex

CCC cortico-cortical coherence

CMC cortico-muscular coherence

DMN default mode network

DSI diffusion spectrum imaging

DTI diffusion tensor imaging

ECG electrocardiogram

EEG electroencephalography

EMG electromyography

FC functional connectivity

fcMRI functional connectivity fMRI

FEF frontal eye fields

FFT fast fourier transform

fMRI functional magnetic resonance imaging

HEOG horizontal electro-oculogram

HPI head position indicator

ICA independent component analysis

IPC inferior parietal cortex

L mean characteristic path length

LFP local field potential

LV latent variable

M1 primary motor cortex

MEG magnetoencephalography

MRI magnetic resonance imaging

MSR magnetically shielded room

MVC maximum voluntary contraction

PCA principle component analysis

PCC posterior cingulate cortex

PET positron emission tomography

PFC prefrontal cortex

PLS partial least squares

PMC premotor cortex

PMCd dorsal premotor cortex

PMCl lateral premotor cortex

PMCMed medial premotor cortex

PMCv ventral premotor cortex

PO parietal operculum

PPC posterior parietal cortex

rCBF regional cerebral blood flow

ROI region of interest

rTMS repetitive transcranial magnetic stimulation

S small-worldness

S1 primary somatosensory cortex

S2 secondary somatosensory cortex

SC structural connectivity

SMA supplementary motor area

SPC superior parietal cortex

SQUIDS superconducting quantum interferences devices

tDCS transcranial direct current stimulation

TMS transcranial magnetic stimulation

tSSS temporal signal space separation

UL upper-limb

V1 primary visual cortex

V2 visual area two

V5 middle temporal visual area

vACC ventral anterior cingulate cortex

VEOG vertical electro-oculogram

ACKNOWLEDEGMENTS

I would like to express my appreciation and gratitude to my primary supervisor Dr. Shaun Boe and my co-supervisor Dr. Timothy Bardouille, for guiding me through this major accomplishment. They are both extremely knowledgeable in their respective fields, and more importantly they are great teachers. By helping me improve upon my weaknesses and by praising my strengths, this process has been an amazing learning experience. Each one has provided me with a different set of skills (analytical, technical, and professional) that I will continue to use in both my future education and my career. Without their patience, guidance, and support I would not have been able to conduct this research and produce a thesis of comparable quality to the present.

Furthermore I would like to thank my other committee member Dr. David Westwood for being a part of this process. By providing insight and recommendations to the project he has certainly enhanced the quality of the thesis. His knowledge and critical analysis of the literature is inspirational, and learning from him throughout coursework, journal club, and my thesis project has been a very positive, educational experience.

I would also like to thank the Nova Scotia Health Research Foundation and the Heart and Stroke Foundation of Canada for funding the current project. Without such funding, a lot research would not be possible and students like me would not have such amazing opportunities.

I would also like to acknowledge my lab colleagues, as they have fostered a fun learning environment for all of us over the past two years. We have all helped each other accomplish our goals, and I wish them luck in their future endeavors.

Finally I would like to show my gratitude to my family, friends, and girlfriend, for their constant support and motivation. Maintaining a work-life balance is important and I am both glad and grateful that these people were there for me the whole way through.

In conclusion, with the support from my supervisors and my family, the past two years have been both extremely educational and fun. I cannot thank Drs. Boe and Bardouille enough for agreeing to take me on as a graduate student and I am grateful for their decision to do so.

CHAPTER 1: INTRODUCTION

Engaging in a motor task results in the activation of multiple, anatomically distinct regions of the brain. This collection of regions, including, but not limited to, the primary motor cortex (M1), primary somatosensory cortex (S1), and supplementary motor area (SMA), collectively form a sensorimotor network. Damage to areas within the sensorimotor network resulting from neurological injury, such as stroke, alters the pattern of activity within the network, most often resulting in physical impairments. Being able to compare a damaged network to a healthy non-disabled network would be useful in determining changes resulting from neurological injury. Therefore it is important to understand what is happening within a healthy brain before conclusions can be made about a damaged or lesioned brain. New techniques in brain imaging have provided ways to examine the functional connections between brain regions, which is one method of examining differences between networks.

The functional connections between distinct brain regions can be inferred by determining the coherence between their activations, defined as a measure of the phase consistency between the two signals at a given frequency. Functional connectivity (FC) analysis is a technique that highlights the synchrony between distinct regions of the brain by examining synchronous cortical oscillations over time. Using FC analysis provides insight into what regions may be communicating during a given task. Once the functional connections are determined, graph theory may be applied to quantify these connections. Graph theory is a mathematical approach to analyzing data based on connections between points on a graph and it characterizes and provides useful information about a dataset.

The goal of the present study was to determine the functional connections between anatomically distinct regions of the brain within a group of non-disabled

participants and then to quantify these network connections. Participants' neural activity was recorded with magnetoencephalography (MEG) while they were at rest and during the performance of a unilateral visuomotor task. Coherence between anatomically prescribed cortical and cerebellar regions was then calculated to determine any significant functional connections between states (rest vs. task), elucidating the task-positive network. Graph theory was then used to quantify these connections. Key regions in the task-positive network were identified based on their number of connections within the network (termed *node degree*).

It was hypothesized that (1) there would be a significantly different pattern of functional connectivity during the task than during rest, (2) functional connectivity would increase predominantly between nodes of the sensorimotor network that are contralateral to the movement, and (3) the SMA would have the highest node degree in the task-related network, proving itself to be a hub between separate neural areas involved in a visuomotor task.

The results of the FC analysis highlighted a significantly different network during task than during rest (i.e., the task-positive network). It was found that regions previously established as components of the sensorimotor network, including M1, SMA, premotor cortex (PMC), and the cerebellum (CB), were functionally connected within this task-positive network. The graph theory analysis found that these sensorimotor network nodes of the contralateral hemisphere, compared to the ipsilateral hemisphere showed a high node degree, indicating their importance within the network. Furthermore the supplementary motor area proved to be a major component within this network (or a *hub*), based on the fact that it had the highest node degree of 13.

The results of the present study have implications for future research. By highlighting the sensorimotor network in a group of non-disabled participants, we have established a baseline or template of neural activity to which the results of future studies may be compared. The present study is the first phase of a larger study that will utilize the same paradigm and analysis procedures to examine network connectivity in a group of patients post-stroke. Future comparison of these two distinct networks will highlight how network dynamics are altered as a result of stroke, informing stimulation-based treatments used in neurorehabilitation.

CHAPTER 2: LITERATURE REVIEW

2.1 An Overview of Neural Communication

It was not until the late 1800's that scientists first proved that nervous tissue is composed of discrete units known as 'neurons'. Using novel cell staining techniques, Ramon y Cajal discovered that a mass of nervous tissue is a complex collection of discrete units, and not a continuous web (Cajal, 1906). This discovery provided the basis of the *neuron doctrine* which states that the nervous system communicates through signaling between individual neurons (Kandel, 2000).

Since the formulation of the neuron doctrine, it has been well established that neurons communicate through both electrical and chemical signaling. However, up until the mid 20th century much remained unknown about how groups of these neurons worked together. Work by Donald Hebb (Hebb, 1949) showed that when groups of neurons fire together repeatedly over time, they eventually strengthen their connections. Over time, via long-term potentiation, co-activation of pre-synaptic and post-synaptic elements of neurons leads to a facilitation of chemical transmission which may last for hours, months, or even years (Cooke and Bliss, 2006). Hebb postulated that instead of having highly specialized 'cardinal cells' that are responsive to very specific stimuli (i.e. one cell for one person's face), there are groups called 'cell assemblies'. These assemblies contain neurons that respond to elementary features of our environment, and they work (or 'fire') together to form a representation as a whole. This synchrony in neural discharge enables learning from an early age, as the brain is able to adapt and form novel connections between cells, forming new assemblies, as it perceives both new and old stimuli. Having massive amounts of cardinal cells to represent every object we see would be highly inefficient and would require millions of cells for stimuli that we have not encountered.

Therefore the formation of assemblies is more efficient and is a potential solution to the 'binding problem', which questions how relationships between separate neurons leads to the integration and representation of complex objects in our environment.

2.2 Synchronous Neural Firing

It has been suggested that distinct neuronal assemblies communicate through synchronous firing which in turn leads to the functional integration of neural events (Milner, 1974, von der Malsburg, 1981, Singer, 1999). Milner (1974) proposed that neurons in the visual cortex that respond to features of the same object should discharge in synchrony whereas cells that respond to different objects should discharge asynchronously. More specifically, it has been shown that when spatially separate regions (i.e., cell assemblies) within the brain are synchronously firing (i.e., oscillating) within the same frequency band, they are believed to be communicating with each other (Fries, 2005). Figure 1 below shows a simple diagram of neural communication through synchronous oscillatory activity.

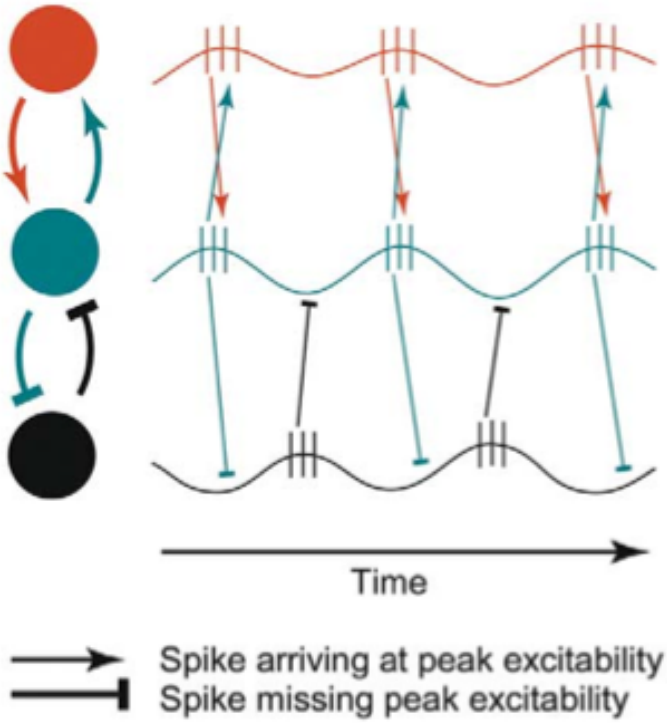

Figure 1. Neural Communication through Synchrony. Each circle on the left represents a separate neuron or cell assembly. The arrows represent facilitation whereas the flat headed lines represent the absence of facilitation. Adjacent to each neuron is a waveform representing its membrane potential. The vertical lines represent the neuron firing (or an action potential). The red and green neurons are active at the same time and with the same frequency. Therefore, communication is facilitated. The black neuron is out of phase and not synchronous with the other neurons. Image taken from (Fries, 2005).

One of the earliest studies to demonstrate neural communication based on neural synchrony investigated the visual cortex of the anaesthetized cat (Gray and Singer, 1989). The authors conducted multi-unit and local field potential (LFP) recordings from areas 17 and 18 of the visual cortex while presenting a visual stimulus (optimally aligned light

bars). The study authors concluded that local neuron populations in visual cortex engage in stimulus specific oscillatory synchronization with a peak frequency near 40 Hz. As a control, single and multi-unit recordings were also obtained from the lateral geniculate nucleus of the thalamus. The control recording showed no synchronous activity between the lateral geniculate nucleus and the visual cortex. The authors state that the neurons involved in generating these synchronous oscillations are confined to a small volume of cortex, and more specifically confined within a single orientation column. A follow-up study (Gray et al., 1989) expanded upon these findings, showing that neurons in spatially distinct regions can also synchronize their oscillatory activity. Using cats, the researchers located two spatially separated neuronal groups in the visual cortex that responded to one long light bar, or two separate, smaller light bars. When the smaller light bars shared the same orientation and were moved in the same direction, synchronous oscillatory activity between the two spatially distinct regions occurred. However no synchrony was found between the two distinct regions when the light bars were moved in different directions. Furthermore, the presence of one long light bar enhanced the synchronous oscillatory activity between these two groups, indicating the ability of separate neuronal groups to synchronize based on the global features of an object such as direction and continuity.

Oscillatory activity is generated by large groups of neurons within a dense system and is concurrent with, and may support, synchronous neuronal firing. The rhythmic activity is generated by neuronal interaction through multiple feedback loops. These loops involve a combination of both excitatory and inhibitory potentials resulting from excitatory pyramidal neurons, inhibitory interneurons, and long-range interactions along the axonal tracts of white matter fibres. Synchronous activity between large groups of neurons is the source of oscillatory activity recorded by various neuroimaging modalities,

including MEG. More specifically, the signal recorded by MEG is created by the summation of the excitatory postsynaptic potentials generated by the dendrites located tangentially to the cortical surface. Depending on the type of loop configuration, oscillations will occur in different frequency bands such as the alpha (9-12 Hz) or beta (15-30 Hz) bands (Bressler, 2002b). Details related to recording neural activity using MEG are provided in section 3.5.3.

2.2.1 The Beta Rhythm is Related to Movement – Motor Unit Synchrony

The beta rhythm is a cortical oscillation that occurs roughly in the 15-30 Hz frequency range, and can be recorded using modalities such as motor unit recording, electroencephalography (EEG) or MEG. It has been established through multiple studies that the beta rhythm is linked to the performance of motor tasks and thus muscle activation (Baker et al., 1997, Feige et al., 2000, Brovelli et al., 2004, Schoffelen et al., 2008). A study by Farmer et al. (Farmer et al.) examined this link by studying the coherence between the firing of hand muscle motor units in healthy controls, as well as patients with central and peripheral neurological lesions. To accomplish this, the participants were asked to maintain a weak isometric abduction of the index finger while recordings were made from 2 separate motor units in the first dorsal interosseous (1DI) muscle of the dominant hand. Using a coherence analysis, the results indicated that there was a significant association between motor unit firing in 1DI in the beta band (16-32 Hz) for healthy controls. Also, the results from a group of stroke patients indicated that when motor unit activity was recorded from the affected 1DI muscle, compared to the healthy participants, there was a complete absence of beta-band coherence between motor units. The authors concluded that central, rather than peripheral, pre-synaptic inputs into the motor neurons might be providing a periodic discharge. They inferred that this central

discharge, in turn, is responsible for the discrete synchronous recordings in the motor units.

2.2.2 Central – Peripheral Neural Synchrony

Several researchers have studied the idea that rhythmic oscillations are driven by central sources and thus have examined the relationship between groups of neurons in the central and peripheral nervous system (Murthy and Fetz, 1992, Baker et al., 1997, Brovelli et al., 2004). Murthy and Fetz (1992) examined coherence between the motor and somatosensory cortices and a peripheral muscle in two awake rhesus monkeys. Using microelectrodes they recorded single and extracellular unit activity, and LFPs from within the motor and somatosensory cortices, as well as electromyographic (EMG) activity from the flexor and extensor muscles of the forearm. They had the monkeys engage in a variety of tasks including retrieving food from a Kluver board, retrieving food from the hand of an experimenter who was out of the field of view, extending and flexing the wrist, and also periods of quiet sitting to observe any spontaneous activity. The authors reported that there were synchronous 25-35 Hz oscillations (which includes the upper end of the beta-rhythm) in LFPs and unit activity while the monkeys performed specific reaching and grasping tasks. Furthermore the authors reported that there was also synchronous modulation between the sensorimotor cortex and muscles of the forearm. Although cortical oscillations were not consistently related to the bursts of muscle activity, cycle-triggered averaging of the EMG signals resulted in synchronous modulation between the muscle activity and LFPs. Briefly, averages of the rectified EMG signals aligned with averages of LFPs did not reveal any consistencies in their timing, due to their spontaneity over time. However, when the cycle-triggered averages were aligned with a particular phase of the LFP cycles, correlated oscillatory activity was

found, indicating communication between the brain and the muscle, which is referred to as cortico-muscular coherence (CMC). This finding provides direct evidence for the link between cortical and muscle synchronous oscillations during a behavioral task.

Following the work by Murthy and Fetz, Baker et al. (1997), also demonstrated that coherence occurs between the cortex and muscle during performance of a precision grip task. In two adult female macaque monkeys, the researchers recorded LFPs as well as pyramidal tract neuron discharge from pairs of sites in M1. The discharge of pyramidal tract neurons was found by electrically stimulating pyramidal tract fibres in the medullary pyramid and recording the antidromic activity at the level of the cortex. Electromyographic activity was also recorded from the hand and forearm muscles (7 muscles total). The recordings were conducted while the monkeys gripped independently pivoting bars between their index finger and thumb and had to retain them in a specified position for 1 s intervals. It was found that there was significant coherence between cortical slow wave signals and EMG activity in all muscles examined for both monkeys. The mean peak frequency exhibiting coherence was within the beta band (25.8 Hz). Again, these results show that during a motor task there is synchrony between beta band oscillations within the motor areas of the brain and the muscles being activated.

2.2.3 Cortico-Cortical Synchrony

A final point, which is most relevant to the present study, is that in addition to central-peripheral communication, researchers have also discovered communication between cortical regions within the beta frequency related to movement. This communication has been termed *cortico-cortical coherence* (CCC). Using monkeys, Brovelli et al. (2004) demonstrated that synchronized beta oscillations in M1 occur during contractions of contralateral arm and hand muscles. Through intracranial

recordings they were able to show that monkeys performing a one-handed motor task had underlying synchronized activity between M1, S1, and inferior posterior parietal cortex (IPC). The study by Brovelli and colleagues (2004) has demonstrated a beta-band sensorimotor network resulting from maintaining a steady unilateral muscle contraction. Several of the studies described above also showed that there is significant coherence between cortical neuronal groups. The study by Baker et al. (1997) showed that there was significant coherence (in the 20-30Hz range) between LFPs and pyramidal tract neuron discharge from pairs of sites separated by a distance of 1.5 mm within M1. Finally, the study by Murthy and Fetz (1992), showed coherent LFPs between distinct regions of M1, as well as between pre-central and post-central sites, separated by an intracortical distance of 20 mm. These findings illustrate both within-region and between-region communication in the brain during motor tasks.

2.2.4 Determining Cortico-Cortical Synchrony with Neuroimaging

Although much of the initial research around neuronal communication used intracortical recordings to study neural oscillations in primates, studies have since used non-invasive imaging modalities such as EEG and MEG, in humans. A key study in this area specifically examining beta band coherence between different brain areas in a group of healthy controls was done by Schoffelen et al. (Schoffelen et al.). In the study, 18 healthy participants performed isometric wrist extensions on both the dominant and non-dominant side (during separate blocks). Extensions were performed against the lever of a force meter and kept constant, between 1.1 and 1.5 N, for a variable amount of time (average of 7s). Whole-head MEG activity was acquired through a 151-sensor axial gradiometer system, and surface EMG was recorded from the right and left extensor carpi radialis longus (forearm) muscles. Coherence was analyzed between both the EMG and

cortical sources using a modified spatial filtering algorithm based on the Dynamic Imaging of Coherent Sources (Gross et al., 2001). Dynamic Imaging of Coherent Sources localizes coherent brain regions using a frequency-based beamformer spatial filter. The authors found that there was significant coherence between EMG signals in the forearm muscle and the contralateral motor cortex in the beta band (median peak frequency was 25 Hz for right hand and 25.5 Hz for the left hand). In a second coherence analysis, they utilized a double dipole model that allows for coherence to be found between the EMG signal and any other regions that may also be correlated, apart from the contralateral M1. This analysis revealed that there was also significant coherence between the ipsilateral CB and the muscle from which EMG was recorded. As well, the authors measured coherence between M1 contralateral to the involved muscle and sources in the rest of the brain to estimate CCC. However, no significant coherence patterns were observed with this CCC analysis. Therefore, this study has again highlighted CMC during a motor task, while failing to demonstrate beta band coherence between cortical regions during a motor task. The authors note that the reason for the lack of observed synchronous neural activity may be to due to a low signal-to-noise ratio, which impacts the quality of source estimates.

A more recent study (Bardouille and Boe, 2012) also used MEG to examine beta band CCC in a group of non-disabled participants. Their task required participants to squeeze two rubber bulbs (held in the left and right hand), to move a cursor toward a target. They concluded that CCC increased predominantly in the beta (16-32 Hz) and gamma (32-64 Hz) frequency bands during task performance, as compared to a resting state. Further, the regions expressing increased coherence with other regions during task performance (i.e., task-related synchrony) were areas previously described as being

important to movement and somatosensation, motor planning, executive control, and vision. Specifically, the authors identified M1, S1, PMC, SMA, CB, prefrontal cortex (PFC), and the frontal eye fields (FEF). However, this study used a bilateral task, rendering it difficult to differentiate cortical activation in relation to the activated limb (i.e., left vs. right). Therefore, further research implementing a unilateral task would be useful. Such a study would enable distinction between activation in the hemispheres that are contralateral and ipsilateral to movement. Regardless, this study highlights that beta band coherence increases between functionally relevant brain regions during the performance of a motor task in non-disabled participants.

2.3 What is a Neural Network?

Although the brain is technically one organ, many regions of the brain appear to be specialized for specific tasks (e.g., M1 stimulation results in movement). These distinct regions and cell populations interact to form *neural networks* that work together to produce cognition and behavior. Therefore the entire brain can be thought of as a network, containing a subset of smaller, specialized networks. The notion of different brain regions interacting as a network is supported by the evidence outlined above showing synchrony between spatially distinct regions of the brain. There are many networks within the brain that communicate to support the performance of various functions. The present study will focus on the sensorimotor network. This network is the combination of brain areas that work in concert to produce movement, including but not limited to M1, lateral (PMCl) and dorsal premotor cortex (PMCd), SMA, and the CB (Kuhtz-Buschbeck et al., 2008, Bardouille and Boe, 2012, Boe et al., 2012, Cheyne, 2013).

2.4 The Brain Is a Network

Due to the complexity of the brain, its biological structure has been compared to that of a computer (Hopfield, 1982). Much like a computer or electrical device is composed of multiple connections created from smaller parts such as wires, the human brain is also composed of multiple connections, on the order of hundreds of billions between neurons (Herculano-Houzel, 2009). Information is transferred across this vast and dynamic network of connections to support the performance of a variety of tasks. The brain has also been described as exhibiting a 'small-world' architecture, in that it is both highly efficient at information transfer, and segregated into distinct specialized 'hubs' of densely connected pathways (Achard et al., 2006). It is believed that, over centuries, the brain has developed to be more efficient, containing the least amount of white and grey matter as possible (Hofman, 2014). This structural evolution enables the brain to transmit information over short distances within smaller hubs or networks, and when required, information may be transmitted between networks through longer but less numerous interconnected pathways.

The connections between neurons, or neuronal populations, are commonly described in one of two ways: structural or functional connections. *Structural connectivity* (SC) refers to a description of the anatomical or physical connections between brain regions (Bullmore and Sporns, 2009). Through these structural connections, the brain forms one large neural network, which receives input from, as well as provides output to, the rest of the body. As well, these connections are used for the transfer of information between brain regions in smaller neural networks. The information transfer or communication between two spatially distinct regions of the

brain, or between the brain and the peripheral nervous system, is referred to as functional connectivity (FC).

2.5 What is Structural Connectivity?

The early method of determining the structural layout of the nervous system was to dissect cadavers and document the anatomical configurations. Although this research still continues, researchers have since developed novel methods to examine the nervous system by using non-invasive imaging modalities. The first complete structural map of a nervous system created using such a method was done on a nematode, through reconstruction of electron microscopy sections (White et al., 1986). This reconstruction was possible due to the simplicity of the organism, which contained 302 neurons, most of which were unipolar. Since this reconstruction, researchers have attempted to map segments of more complicated nervous systems. For example, the cortico-thalamic system of the cat (Scannell et al., 1999) and the cerebral cortex of the macaque (Young, 1993) have been mapped.

More recently, researchers have attempted to non-invasively create a complete map of SC in the human brain through the human *connectome* project (Sporns et al., 2005). This project uses both diffusion tensor imaging (DTI), as well as diffusion spectrum imaging (DSI; Guye, 2008). Diffusion imaging works by measuring and determining the magnitude and direction of the way water molecules diffuse through biological organs using magnetic resonance imaging (MRI). This diffusion reflects the orientation of white matter fibres in the brain (Guye et al., 2008). One study by Hagmann and colleagues (Hagmann et al., 2007) mapped the whole-brain of two participants at a millimeter scale using DSI, resulting in a 3-dimensional reconstruction which contained over 1.5 million fibres. In accordance with previous imaging and retrograde tracing

research, they found connections between separate visual areas (e.g., primary visual cortex (V1), visual area two (V2), middle temporal visual area (V5)) as well as long-range connections such as those between the optic radiation and the lateral geniculate body, and between V2 and V5. This study, using DSI, was able to non-invasively highlight structural pathways within the brain, regardless of their respective functions.

2.6 What is Functional Connectivity?

Functional connectivity refers to the communication between spatially distinct regions of the brain, as measured through coherence between oscillatory activity. Functional connectivity has been more broadly defined as "the temporal correlation of a neurophysiological index measured in different brain areas" (Friston et al., 1993). For the purposes of the present study, coherence is defined as a measure of the phase consistency between two signals at a given frequency, which is based on a consistent phase shift between the signals over repeated measures (Nunez et al., 1997). Functional connectivity along structural connections is an important topic for the present study. Several of the studies described above that used multi-unit recordings to measure spike trains of activated neuronal groups were actually applying a basic form of FC analysis. By using cross-correlational analysis, the researchers determined the synchrony between time courses of activation in spatially distinct neuronal populations (Murthy and Fetz, 1992, Baker et al., 1997). However, recording directly from specific neuronal populations with microelectrodes is impracticable for human studies. As such, many human studies of FC focus on brain activity measured non-invasively through modalities such as positron emission tomography (PET), MEG, and functional MRI (fMRI).

2.6.1 Functional Connectivity using PET

One early neuroimaging study that examined FC in a group of healthy controls, was done using PET (Friston, 1993). The study consisted of a sample of six participants, who underwent 12, 2-minute scans, separated by an interscan interval of 8 minutes, while performing a verbal task. All data was spatially normalized (using the Talairach and Tournoux system), time-locked to the task and averaged across the group. A recursive principal component analysis (PCA) was then conducted on the brain regions that showed a significant difference in regional cerebral blood flow (rCBF). Principle component analysis extracts components from the dataset that account for the variance within the dataset. Regions that were contained in the same principle component were considered to be demonstrating FC. The author's results indicated that several spatially distinct regions were functionally connected during the verbal task. These regions were the anterior cingulate, the left dorsolateral prefrontal cortex, Broca's area, the thalamic nuclei, and the CB. These regions were in agreement with previous literature about brain areas involved in the generation of words and were previously shown to have dense and reciprocal structural connections.

Although PET imaging has been used in the past for doing FC analysis, it is not the optimal modality for doing such analyses. By tracing a radioactive agent that is injected into the bloodstream, PET images the human brain by determining brain areas in which rCBF has changed. It is assumed that changes in rCBF occur because those regions are utilizing oxygen due to increased neuronal activation. As such, PET is an indirect measure of brain activity. Another important point is that the temporal resolution of PET functional imaging is on the order of minutes. Thus, PET is likely to be missing a large amount of neural processes that occur on the millisecond time scale. Due to its nature, FC

analyzes data over time, therefore it is important to use a high temporal resolution modality to capture as much information as possible.

2.6.2 Functional Connectivity using fMRI

Functional MRI has also been used to analyze FC during both task performance and at rest. Research has shown that FC can be assessed using fMRI by measuring interregional correlations between Blood Oxygen Level Dependent (BOLD) signals over time. The underlying assumption is that synchronous BOLD activity in separate brain regions is indicative of information transfer between these regions. However, fMRI faces the same issues as PET imaging. By recording the BOLD signal, fMRI also indirectly measures neural activity (Ogawa et al., 1990). Also, although the temporal resolution is not as poor as PET, fMRI can only record the brain's response on the order of seconds, which is not adequate to capture brain activity occurring on the order of milliseconds.

One study (Honey et al., 2009) attempted to uncover a possible relationship between SC and FC within the human brain at rest, as well as to assess the reliability of FC across scans (two separate scans) using fMRI. The researchers obtained resting state fMRI data on five participants and structural maps using DSI. Resting state FC was calculated by finding the Pearson correlation coefficient of the BOLD signal between 998 regions of interest (ROIs). This study produced several useful results to consider within the context of SC and FC research. First, the authors found that it is not possible to infer SC from FC. When there was a direct structural connection between the ROIs, there was a higher correlation between SC and FC. However, as the distance between regions increased, SC tended to decrease while FC often remained. This highlights the major differences between SC and FC analyses, and provides evidence that although most structurally connected regions are functionally connected, SC does not always predict FC.

This is important as it showed the ability of FC analysis to locate non-directly connected, spatially distinct regions that are showing synchronous activity over time.

Furthermore, FC did not exhibit intersession reliability for any of the participants, within and across scanning sessions. The authors note that this could be due to a reconfiguration of neuronal interactions, the result of signal components of an unknown origin, or possibly a combination of the two. These findings are important because they pose the possibility that determining FC through fMRI may not be an ideal approach. Perhaps a more direct measure of neural communication should be used when performing FC analyses? Using an alternate modality that directly records neural activity and provides more useful information, such as the frequency of cortical oscillations may provide more insight into the underlying neuronal communication.

2.6.3 Examining FC at Rest: the Default Mode Network

Previous research has discovered a resting state network, which is known as the "default mode network" (DMN). It is known that regions within this network exhibit increased activity when participants have their eyes closed, are at rest and are not thinking of anything in particular. Functional connectivity within this network has been demonstrated multiple times using a myriad of modalities (for a review see (Broyd et al., 2009). One particular fMRI study (Greicius et al., 2003) provided insight into how FC in the DMN changes between rest and task. The paradigm required 14 healthy participants to perform a resting block first, followed by three different tasks: a passive visual processing task, a visuospatial working memory task, and a face-processing task (which was not included in their analysis). Data from the working memory task and rest block were used in conjunction with a random-effects analysis to establish the ROIs with either decreased or increased activity during task performance. To determine the ROIs that were

functionally connected, the average time series of all voxels in each ROI were used as a covariate in a whole-brain, linear regression, statistical parametric analysis. A second random-effects analysis was then used to determine which regions showed FC across subjects between the resting state and the visual processing task. It is important to note however that each analysis was done independently, resulting in two separate task-related FC analyses. It was found that both the posterior cingulate cortex (PCC) and the ventral anterior cingulate cortex (vACC) were functionally connected during rest and they also decreased in activation during the working memory task (as previously shown). Interestingly, during the visual-processing task, the FC analysis revealed an identical change, proving that PCC and vACC were important components of the DMN. Based on the results, this study demonstrates that when the brain moves from rest to performing a task, the functional changes within brain networks can be highlighted using non-invasive neuroimaging.

2.6.4 State-Related FC

A novel approach to FC analysis, as described in the previous example, is to compare neural connectivity between different states, which is referred to as *state-related FC*. By determining FC between multiple brains regions during two different states, comparisons can be made concerning any change in synchrony as a function of state. State-related FC analysis reveals any significant increase or decrease in connectivity based on condition, and has been used to examine the change in FC between a rest and task condition, demonstrating what is referred to as the task-positive network. To date there has been limited research examining task dependent changes in FC networks. The study by Bardouille and Boe (2012) described above utilized a state-related approach. Based on MEG data, the CCC between 80 pre-determined regions was calculated during

both rest and task. A partial least squares (PLS) analysis was then done to determine any significant differences in CCC between states. This method highlighted both a task-positive and task-negative network. Their results indicated a functionally connected sensorimotor network that is significantly more synchronous during task than rest.

2.7 Functional Connectivity with MEG

Much like fMRI and PET, MEG data can be utilized for FC analysis. Several studies have demonstrated MEG's ability to determine coherence between spatially distinct regions of the brain within specific frequency bands (Bartolomei et al., 2006, Bassett et al., 2006, Bardouille and Boe, 2012). By directly assessing neuronal activity within separate regions of the brain on the millisecond time scale, MEG lends itself as the perfect modality for performing such analyses, and these benefits will be described below.

2.7.1 Neural Basis of MEG

MEG was inspired from studies that recorded the magnetic fields produced by organs of the body, such as the heart (*magnetocardiography*, for a review see (Hart, 1991). It is from here that researchers began recording components of the magnetic fields produced by the brain, as a function of time, termed *magnetoencephalograms* (Cohen, 1972). According to Ampere's law, when current flows through a wire (or in this case a neuron), it produces a magnetic field surrounding that wire. When presynaptic neurons activate the postsynaptic neuron, they cause postsynaptic potentials, which are characterized by a current flowing through the apical dendrites. This effect is amplified by a large factor because the white matter tracts in the brain contain millions of neurons bundled together, that fire roughly simultaneously. When large groups of neurons that are tangential to the skull are activated, the MEG scanner detects the strength and location of

these magnetic fields produced based on Faraday's Law of magnetic induction. The magnetic fields produced from the brain, induce a current within the coiled wire in the MEG sensors, which is subsequently converted to voltage at each sensor location. The recorded field strength is indicative of neural activity. (Cohen, 1972). Figure 2 below shows how the magnetic fields produced in the brain project outside of the skull.

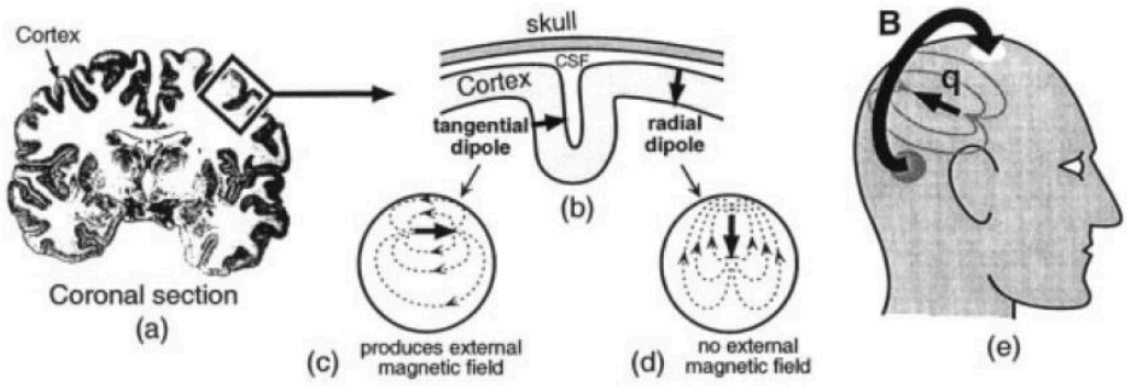

(Vrba, Robinson, 2001)

Figure 2. Sources of magnetic fields from the brain. a) A coronal section of the brain. b) Magnified view of the cortex from the coronal section, showing a gyrus and sulcus. Current dipoles can be used to model the electrical neuronal activity that is tangential (c) or radial (d) to the skull. e) The activity from a tangential current dipole produces a magnetic field that projects perpendicular to the surface of the head, which is recorded by the MEG sensors. Image from (Vrba and Robinson, 2001).

2.7.2 MEG Technology

Along with its advantages, MEG has several limitations. However as MEG technology improves, so does the quality of the data obtained. One major problem with MEG imaging is that the magnetic fields generated by the brain are on the order of 10-100 fT, which is a billion times smaller than the earth's magnetic field. Anytime MEG

data is being recorded, other magnetic fields produced from sources outside of the head are also recorded. In fact, the MEG scanner is capable of recording the current in nearby power lines, magnetocardiography and other biomagnetic signals, and moving objects such as elevators or cars. In an attempt to reduce these artefacts, several hardware improvements have been introduced or improved. The MEG system used in the current work consists of triplet sensor arrays composed of two different super conducting sensor types: planar gradiometers (2 per location), and magnetometers (1 per location). The planar gradiometers are composed of two oppositely wound coils that measure a change in magnetic field (or flux) across the coils. In addition to recording sources from the head, they also reject any environmental noise, which should theoretically be constant across the coils, resulting in a flux of zero, thereby detecting only changes in magnetic field strength generated by the head. The magnetometers consist of only one wound coil, and are sensitive to deeper sources than the planar gradiometers, albeit they are also prone measuring external noise. It is this combination of coils that filters environmental noise from the signal and sends changes in magnetic fields to Superconducting QUantum Interference Devices (SQUIDs) in the form of electrical current. The SQUIDs then convert this current to a voltage and this is how neural activity is recorded. To further try and eliminate environmental artefacts, the MEG scanner is housed inside a magnetically shielded room (MSR). The MSR is made of multiple layers of mu-metal (a ferromagnetic material), copper, and aluminum that *passively* filters external noise. It also *actively* filters out external noise by creating a current opposite to that of the environment, by recording signals that penetrate the MSR using a subset of the magnetometers (Baillet et al., 2001).

2.7.3 Comparing MEG to Other Modalities

As outlined in previous sections there are a number of other commonly used modalities for functional neuroimaging in both non-disabled controls and clinical populations including PET, MEG, EEG, and fMRI. It is important to note that each modality has strengths and weaknesses due to the differences in both the source of neural activity they record, and the means in which the signal is recorded. The most important benefit of MEG in comparison to EEG is spatial resolution. Both MEG and EEG face the difficult problem of identifying neural sources based on signals recorded outside the brain, termed the *inverse problem* (Lamus et al., 2012). Compared to MEG, EEG has a lower spatial resolution for an equivalent sensor array density because the thick, conductive layer of the skull spatially smears the electric potentials it records. The magnetic fields recorded with MEG are not strongly affected by the skull, so sources can be localized with greater accuracy. Also, fluctuations in the impedance of EEG electrodes over the course of the scan can introduce a potential artefact in the recorded signal (Kappenman and Luck, 2010).

The main advantage of MEG, as compared to fMRI, is temporal resolution. Having the ability to record direct correlates of neural activity with millisecond precision gives MEG an advantage in temporal resolution over fMRI, which records a slower (~1s) neurovascular response. Many neural responses occur less than 1 second after the presentation of a stimulus. In fMRI recordings, these responses are temporally smeared together and the "order of operations" cannot be determined. Therefore, it is important to be able to record with millisecond temporal resolution. Also it is important to note that fMRI measures changes in blood flow to regions of the brain that are active during a given task. As such, fMRI is an indirect measure of neural activity (Ogawa et al., 1990).

The magnetic fields produced by the brain, however, are directly caused by neuronal activation.

2.8 What is Graph Theory?

As described above, FC analysis highlights the communication between neural regions underlying the performance of a motor task. While determining the synchrony between regions is useful there is a need to quantify and characterize network parameters. Once functional connections are determined between separate brain areas, within specific frequency bands, these connections can be quantified using graph theory, which is a tool for characterizing networks. Within the world there exists a large number of diverse and complex networks. These may take the form of social networks (e.g., a person's group of friends), artificial networks (e.g., network connections established through the internet), and biological systems such as the connections between separate brain regions, among many more. On a macroscopic scale, all of these complex systems share key organizational principles that can be quantitatively characterized by a set of pre-established measures or parameters (Bullmore and Sporns, 2009). These measures are based on the mathematical study of networks, known as *graph theory*. Within graph theory, a network is defined as a mathematical representation of a real world network. The mathematical representation is composed of vertices called "nodes" that are interconnected through "edges" (Rubinov and Sporns, 2010). There are several classifications of edges, determined by their direction and weight. An edge may be undirected, which is denoted by the presence of one connection between two nodes, irrespective of direction of information flow. Alternatively an edge may be directed which means that a connection begins at node *i* (output) and ends at node *j* (input), and is only considered to send information from *i* to *j* and not vice versa. An edge may also be

weighted meaning that the strength or reliability of the connection is quantified. Alternatively, an edge may be unweighted meaning that it is quantified using a binary system (i.e., a connection = 1, no connection = 0). Using these measures a neural network may be weighted-directed, weighted-undirected, binary-directed or binary-undirected (this being the simplest form of a network). It is believed that graph theory originated from a problem titled 'the bridges of Konigsberg', illustrated by mathematician Leonard Euler. In order to prove that one could not traverse the town of Konigsberg by crossing each of the seven bridges once, Euler drew a "graph" to represent the city and its multiple bridges (Stam and Reijneveld, 2007).

2.8.1 Complex Networks are Small-World Networks

Since the discovery of graphs, they have been analyzed using multiple measures and many similarities between networks have emerged. One important discovery was that complex networks often exhibit "small-world" characteristics. These networks contain a high local clustering of nodes (i.e. nodes have many shared connections), paired with short path lengths between nodes, where shorter paths indicate a more efficient network (Humphries and Gurney, 2008). The first demonstration of small-world architecture was shown experimentally by Milgram (Milgram, 1967). The goal of his experiment was that each of his randomly chosen Nebraskan participants (N=160) had to send a letter to a specific target person in Boston (everyone had the same target). However the caveat was that the letter could only be sent to a person the participant knew on a first name basis that they thought might know the target person, or a person closer to the target. Milgram then analyzed the data based on *chain length*, that is the number of intermediate persons between the starting person and the target. The results show that the median chain length for each letter was five, and had a range from 2-10 intermediates. This result is surprising

because as the study predicts, the chance that any two randomly chosen people in the United States would know each other is 1 in 200,000 (.0005%). One methodological issue was that of the 160 original letters sent, 126 were dropped. Milgram hypothesized that some were dropped due to lack of a connection to complete the task as well as failure to comply; therefore the average chain length may be longer. Regardless, based on this study, it is evident that human social networks are complex, small-world networks.

2.8.2 What are Specific Network Measures?

One of the more useful network measures used in graph theory is determined by finding how many connections a given node has with other nodes, termed *node degree (Figure 3 a).* Logically it can be assumed that a node in a network with the highest degree can be thought of as having great importance within the network. In the context of neuroimaging, a change in node degree within an area of the brain may be indicative of neural reorganization after task practice or perhaps after a neurological injury. When a node is connected to another node, they are termed *neighbors.* A *cluster* is formed when the neighbors of a node are also neighbors of each other (Bullmore and Sporns, 2009). The *clustering coefficient* (C, Figure 3 b) is the ratio of the number of connections between neighboring nodes (i.e., clusters) to the maximum number of possible connections (Watts and Strogatz, 1998). It is expected that a complex network would exhibit a high clustering coefficient, whereas a random network should exhibit a low clustering coefficient. The *mean characteristic path length* (L) is the average path length across a network, where path length is a measure of the shortest number of edges that have to be traversed to reach a given node (Figure 3 c). For example, in the figure, node A is connected to node B through two nodes, giving a path length of 3. Network efficiency is inversely related to path length (Bullmore and Sporns, 2009).

Another important measure, which has briefly been described above, is the *small-worldness* (S) of a network. Small-worldness can be calculated by finding the ratio between the C and the L of a network (C_N and L_N), as compared to values for C and L generated from a random network (C_{Rand} and L_{Rand}) using the following equation; $(C_N/C_{Rand}) / (L_N/L_{Rand})$ (Humphries and Gurney, 2008). The definition for a small-world network implies that the real network will have a much greater C than the random network; $C_N/C_{Rand} >> 1$, and the real network will have a L no less than that of a random network: $L_N/L_{Rand} \geq 1$. Therefore a small-world network should have an $S > 1$, indicating an efficient network composed of clusters of nodes interconnected by short paths (Watts and Strogatz, 1998). For example a network with $S = 4$ would be considered more small-world than a network with $S = 1$.

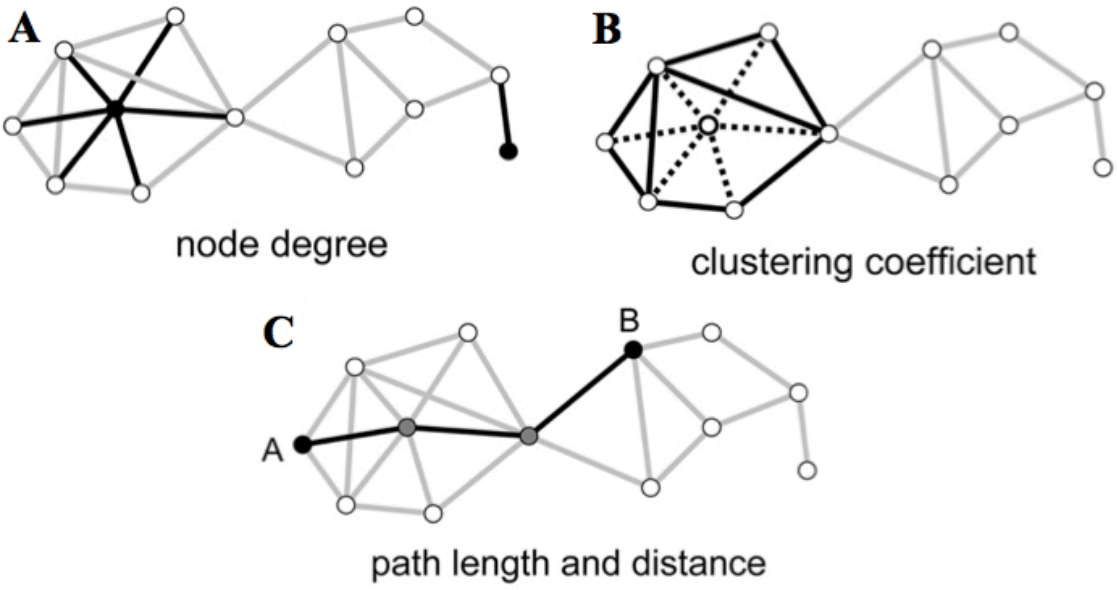

Figure 3. Schematic Diagram of Graph Theory Metrics. A) Node degree. The central node on the left of this diagram has a degree of 6, indicated by connections (thick black lines) to other nodes. B) Clustering coefficient. The central node in this diagram has 6 neighbors (connections) indicated by dashed lines, who have a total of 8 connections

(solid lines) out of a possible 15. Therefore the central node's clustering coefficient is 8/15 = 0.53. C) Path Length and Distance. Between nodes A and B, there are 2 intermediate nodes, giving a path length of 3 between them. From (Sporns, 2011).

2.8.3 Converting Neuroimaging Data into a Graph

Although the mathematical study of graphs has been ongoing for some time, more recently graph theory has been applied to neuroimaging data in an attempt to quantify patterns in brain activity. This application will further help us understand the complex nature of neural communication. Using data obtained from various neuroimaging modalities, nodes can by defined by ROIs, and edges can be defined based on connections either structurally (via white matter tracts) or functionally (through temporal correlations in activity). The data can then be examined in the context of a graph, and network analytical measures can be applied.

2.8.4 Applying Graph Theory to Neuroimaging Data

The first example of a graph theoretical application to neuroimaging data was on the anatomical structure of a worm (Watts and Strogatz. 1998). Watts and Strogatz converted the worm's anatomical network into a graph consisting of 282 nodes with an average of 14 edges per node. An edge was defined as two neurons being connected by either a synapse or gap junction. In order to calculate whether the network was a small-world network, the authors had to find the L and C of the actual network. They then found the L and C of a random network by generating a network with the same number of nodes that had a specific probability of edges between node pairs. Although the L_{actual} (2.65) and L_{random} (2.25) were similar, the C_{actual} (0.28) was much greater than the C_{random} (0.05). The ratio of C/L produces a value >>1, indicating a small-world network. This study was the first that established a neural network as being a small-world network.

2.8.5 Graph Theory Applied to Human FC Data

Studies have since been conducted on human participants and have applied graph theory to FC data. One such study (Bassett et al., 2006) calculated a variety of graph theory measures from MEG data obtained from 22 healthy controls. The participants were either performing a dominant (right) handed finger tapping task (N=11) or an eyes-open rest block (N=11). The dataset was divided into six specific frequency bands that ranged from delta to gamma (1.1Hz - 75 Hz). They calculated average node degree, C, L, and an S value for each band, for both conditions. The results indicate that across all frequency bands as well as between conditions the measures are consistent with and characteristic of a small-world network. Surprisingly, there were no major differences between conditions, apart from the presence of longer paths between frontal and parietal regions within the beta and gamma bands during motor task performance. These results pose the possibility that both the resting state network as well as the motor network are both efficient, small-world networks. Another study that applied graph theory to FC was conducted by Bardouille and Boe (2012). Using MEG they determined FC within the beta and gamma frequency bands in the sensorimotor network while participants performed a bilateral upper limb task. After the functional connections were elucidated, graph theory was used and node degree for each region of interest was calculated. The results showed that regions of the sensorimotor network such as the SMA and M1 expressed a high node degree.

2.8.6 Graph Theory and Clinical Populations

Graph theoretical analysis has the potential to be a clinically beneficial tool. By quantifying changes in FC via graph theory between two networks, researchers can compare networks in healthy non-diseased brains to patient's brains. One study

(Bartolomei et al., 2006) compared the brains of 15 healthy controls to the brains of 17 patients who had either a left or right hemisphere tumor. One of the major purposes of the study was to determine if a tumor results in a decline in the small-world architecture that accompanies a complex neural network. Using MEG, neural activity was recorded during an eyes-closed no-task state for all participants. The authors used a synchronization likelihood measure to determine FC, which statistically determines any interdependencies between brain regions during two time series. Using the MEG channels as nodes, they then created a binary-undirected matrix representative of any connectivity between 149 pairs of nodes. The C and L for both participant groups were calculated for the gamma (26-60Hz), beta (13-25), alpha (9-12Hz), theta (4-8Hz), and delta (0.5-4Hz) frequency bands. Although the results are difficult to interpret as there were differences related to the side of the tumor, there was a decline in small-world architecture in the patient group. Within the theta and gamma bands, the ratio of C/C_{random} was lower for patients with right-sided tumors than for controls. Also in the theta band, beta band (for left sided tumors) and gamma band (for right sided tumors) there was a decrease in the ratio of $L/L_{random,}$ for patients as compared to controls. A random network configuration is characterized by low ratios for both the C/C_{random} and the L/L_{random}. These results demonstrate that FC in the damaged brain is closer to a random network in that it is not as highly clustered as the healthy brain's network and the path lengths are longer. This may help explain the fact that patients with brain tumors exhibit deficits not directly related to the location of the lesion. There is an overall functional alteration within the brain, possibly because its efficiency as a complex network is reduced.

Graph theory has also been used to examine the small-world properties of patients with schizophrenia. Micheloyannis et al. (Micheloyannis et al., 2006) used the

synchronization likelihood measure to determine the FC in healthy controls, and patients with schizophrenia who were stable enough to work and currently taking medication. Electroencephalography scans were done while patients were either at rest or performing a variety of cognitive tasks, including a two-back working memory task. Compared to controls, during the working memory task the C/C_{random} ratio was lower for the schizophrenia group in several frequency bands (alpha, beta, and gamma). Also at rest, the L was higher in the schizophrenia group in the alpha band, as compared to the control group. Although the results vary between condition and frequency band, the study shows that the schizophrenic brain is closer to a random network than the healthy control brain.

Combining these two aforementioned studies, we can see that both a tumor and a psychological disorder are capable of disrupting the 'standard' pattern (as shown by healthy controls) of communication within the brain. This in turn changes the functional connectivity of the brain, resulting in a neural network that has the tendency to be closer to a random network, and not a highly efficient complex small-world network.

2.9 Imaging the Motor Network – Early Research Into Functional Localization

One of the major discoveries that helped establish the motor network that has been imaged and described above occurred in the 1930s (Penfield, 1937). Over a 10-year period, Penfield and Boldrey (1937) conducted microelectrode stimulation on the cortical surface of 196 patients who were undergoing neural surgery. While the cortex was exposed, they would stimulate various regions adjacent to the central sulcus (along the motor and sensorimotor cortex), while increasing the stimulation strength until a positive behavioral response was observed. Any response that was reproducible was then marked by laying a piece of paper on the brain's surface at that point. It is important to note that this research was focused on only motor and somatosensory responses. Their results

indicated a very large number of regions on the cerebral cortex responsible for evoking sensation and movement over the entire body, including the tongue, face, feet, and hands. This study provided important insight into the role of various cortical regions (most importantly M1) and has informed much of neurophysiology literature since that time.

2.9.1 Imaging the Motor Network – The Importance of the SMA

We know the brain is a network so it is important to understand how multiple brain areas work together to produce movement or sensation. A large body of neuroscience research now shifts its attention from specific focal regions to examining FC during somatosensation and movement. As outlined above, using modern neuroimaging technology it is possible to have a participant voluntarily perform a movement and non-invasively record neural activity at the onset of that movement (i.e., an event-related analysis) or throughout the movement (i.e., a state-related analysis). This recording ability enables the recording of changes in activity of multiple regions simultaneously over a specified time interval. Of the many regions composing the sensorimotor cortex, one study highlighted the importance of the SMA in voluntary movement using neuroimaging technology (Orgogozo and Larsen, 1979). Using PET imaging, the researchers had five participants perform various motor actions such as performing complex hand or foot sequences, simple repetitive foot motions, counting aloud, and finally counting mentally (no movement condition). They recorded CBF to the SMA among other regions and found that during each different motor activity there was an increase of CBF to the SMA in addition to the sensorimotor cortex. However, during the mental counting task blood flow was not increased to the SMA, highlighting its importance to tasks that require movement, irrespective of complexity. Although this experiment used patients who experienced focal epileptic seizures, it did use a

neuroimaging modality to image the brain during movement and several studies have since confirmed the role of the SMA in movement (Roland et al., 1980, Shibasaki et al., 1993).

2.9.2 Imaging the Motor Network – The Importance of Laterality

Due to the complexity of the brain, it is important to note that different behavioral tasks may result in activation in different regions of the brain. For example a task that requires moving the lower extremities will elicit different neural activation than a task that requires the upper-limbs (ULs) (Kapreli et al., 2006). Activation patterns also depend on task complexity (Rao et al., 1993), and on the side of the body performing the movement. Many studies have demonstrated that there is a relationship between brain activity and the side of the body that moves using modern neuroimaging technology. For example, Kim and colleagues (Kim et al., 1993) used a 4T MRI to obtain a higher signal-to-noise ratio as well as better spatial resolution than PET imaging for mapping the motor network. For the study, six participants (five right handed and one ambidextrous) were required to make repetitive opposition movements between the thumb and four fingers using either hand (separate conditions) or both hands together (bilaterally) while activity was recorded from right M1 only. The authors found that the activated region was similar for contralateral (left) and bilateral (both) hand movements, but the activated area was 20 times smaller for ipsilateral (right) hand movements. The intensity of activation for each voxel was generated by finding the difference between average baseline and task-induced activity, with results showing that the intensity was 2.3 times greater in the contralateral condition. Although results of this study were limited in that it only explored a single region within one hemisphere, it did highlight the importance of the contralateral M1 in a simple behavioral paradigm.

Other studies, including one by Grefkes et al. (Grefkes et al.), have also demonstrated the lateralization of neural activity using whole-head imaging. For this study, participants (N =14) performed whole-hand fist closing movements at a rate of 1.5 Hz with either their dominant, non-dominant, or both hands (three separate conditions) during imaging with fMRI. Compared to rest, the visually paced hand movements activated the extrastriate visual cortex, sensorimotor cortex, SMA, PMC, inferior precentral sulcus, the secondary somatosensory cortex (S2), and the thalamus. More importantly, the right-handed movements primarily activated left hemispheric areas and the left-handed movements primarily activated the right hemisphere. Also, compared to unilateralized movements, the bimanual condition significantly increased activation in the SMA. Again we see the SMA's importance in tasks requiring UL movements, as well as the predominant contralateral motor network activation. This lateralization provides information for researchers to use during experimental design. Depending on the specific hypothesis and expected regions of activation, choosing the proper task is of critical importance.

2.9.3 Imaging the Motor Network – Differences Between Unilateral and Bilateral Movements

As discussed above, the patterns of brain activity change resulting from movements from the dominant or non-dominant limb independently. Furthermore, it has also been shown that patterns of brain activation significantly change between a unilateral and a bilateral task. Specifically, the resulting activity from a bilateral task is not simply the superposition of the results of two separate unilateral tasks using each limb (Carson, 2005). There are underlying complex interactions that involve inter-hemispheric excitation and inhibition to successfully perform a given bilateral motor task. As an

example of this inter-hemispheric inhibition, research has shown that muscle activity is temporally decreased when transcranial magnetic stimulation (TMS) is applied to the ipsilateral M1 of participants who are maintaining a tonic contraction (Ferbert et al., 1992). This inhibitory mechanism between the motor regions ensures that the opposite upper-limb does not mirror movements from the active limb. This is also confirmed by the finding that during bilateral mirror movements of the wrist, this inhibition is suppressed (Stinear and Byblow, 2002). Furthermore, neuroimaging studies have revealed differences in neural activation between performing the same task with a single limb or both limbs. One study (Sadato et al., 1997) used PET imaging to show differences within the SMA and PMC during finger movements. Participants were required to perform repetitive index finger abduction-adduction movements during a left only, right only, bimanual mirror or bimanual parallel condition. The authors note differences in regional activation across all conditions used. The right index finger activated the left sensorimotor cortex (composed of the S1 and M1), the SMA and the right CB. The left finger movements activated the right sensorimotor cortex, the anterior cingulate gyrus, the posterior SMA, left PMCv, and left CB. The bimanual movements activated the sensorimotor cortex, basal ganglia, inferior parietal lobe and thalamus bilaterally as well as the right prefrontal cortex. Furthermore, the right PMCd and right SMA showed significant activation during the parallel movement compared to the mirror movement. The authors argue that SMA is required for the synchrony of bimanual movements and for the bimanual coordination of parallel movements. They also posit that the PMCd is responsible for integrating information responsible for sequential finger movements between different limbs. These results highlight the widespread differences in neural activation that occur between unilateral and bilateral movements. Another study

that examined changes in neural activation during the performance of bilateral and unilateral motor task used fMRI to examine changes resulting from a sequential finger-tapping task (Nair et al., 2003). Subjects performed a sequential finger-tapping task with both hands separately (2 conditions) or both hands simultaneously (1 condition). The results showed that activity during bilateral movements compared to the left-handed movements was greater in the left sensorimotor cortex, bilateral superior parietal lobes, SMA, and the bilateral CB. Significant differences were also found between bimanual and right-handed finger movements as indicated by enhanced activity in the right sensorimotor cortex, SMA, left precuneus and bilateral CB. Furthermore there were significant differences in activation between the left and right only conditions. Based on these results it is evident that the patterns of brain activation change between bilateral and unilateral movements, and more importantly the changes are different depending on the limb performing the activity.

These aforementioned studies highlight the fact that there are complex interactions between brain regions depending on the nature of the task (bilateral vs. unilateral). This is an important point to consider when designing neuroimaging paradigms. In order to isolate the activation resulting from a single limb on one side of the body, the experiment must require the use of that limb only. One cannot measure brain activity during a bilateral motor task and segregate limb-specific lateralized activity because bilateral movements produce different results than the combination of unilateral movements alone.

2.9.4 Imaging the Motor Network – Neural Changes Based on Varying Grip Task

Not only does the side of the body used result in different patterns of neural activation, but the type of task performed also produces significantly different activation

patterns. To date several studies have examined the changes in brain activity between a precision grip task and a power grip task. One such study (Ehrsson et al., 2000) compared neural activity using fMRI while non-disabled participants (N=5) performed either a precision grip or a power grip task with their dominant (right) hand. A power grip is characterized by a palmar opposition grasp where the digits flex around the object for stability and force (Napier, 1956, Ehrsson et al., 2000). A precision grip is defined as gripping an object between the flexor aspects of the fingers and the opposing thumb (Napier, 1956). The authors found that both grips elicited significant activity in the primary sensorimotor cortex (defined by Ehrsson et al. (2000) as "the cortical motor areas with the exception of the cortex in the depth of the central sulcus") contralateral to the grasping hand, PMd, postcentral sulcus, ventral premotor cortex (PMCv), precentral gyrus, cingulate sulcus, contralateral parietal operculum (PO) and left thalamus. Also, compared to precision-grip, during power-grip there was significantly stronger activity in the contralateral S1, M1 and PO. Another study (Takasawa et al., 2003) used PET imaging with a similar paradigm except the participants (N=7) did not squeeze an object when gripping. Rather, they only performed the movement. Their results indicated that there was no observable difference in neural activity between the two tasks. These mixed results then prompted another study (Kuhtz-Buschbeck et al., 2008) that also used fMRI and a similar varying grip task. Participants (N=14) were required to repetitively squeeze a non-flexible force transducer with their dominant (right) hand using either a power grip or a precision grip. The task was further divided into an eyes-closed condition or a visual feedback condition that showed percentage of maximum voluntary contraction (MVC). During the eyes closed condition, the precision grip task activated the left M1/S1, left dorsolateral PMC, the SMA, bilateral CB, and bilateral foci in the insular and opercula

cortex. The power grip task activated the same regions as the precision grip as well as the thalamus, basal ganglia, and the right supramarginal gyrus bilaterally. The visual feedback condition also activated the same regions, as well as bilateral activations of the occipital and bilateral posterior parietal areas. There were no brain regions more active during the precision condition but the power grip task caused significantly greater activation in the left precentral gyrus and the right CB. The authors also report a positive linear increase in activity along the left central sulcus and the right CB with increasing grip force. Despite previous discrepancies in brain activation between two grip tasks, Kuhtz-Buschbeck et al. (2008) have shown in a relatively large sample that there are in fact differences in activation dependent on the task used. More related to the present study they have also highlighted several areas involved with a unilateral upper-limb power grip task.

In addition to the literature showing a difference between regions activated depending on the task used, studies have also shown that different tasks are associated with distinct patterns of neural oscillatory activity. One study used MEG to demonstrate that varying degrees of force result in different synchronous oscillations between the muscle used and contralateral M1 (Brown et al., 1998). To accomplish this, participants performed weak (20-40%) and maximal (100%) voluntary contractions of their right wrist and ankle (against a plastic restraint) while EMG (from the active muscle) and whole-head MEG were recorded. Coherence and time domain analyses were conducted to determine synchrony between the muscle and contralateral Rolandic area of the brain. The authors conclude that during weak contractions of both limbs, there is a clear peak in CMC within the 20-30 Hz (beta) frequency band. During maximal voluntary contractions of both limbs, the peak in coherence moved to the 35-60 Hz range. Notably, this was one

of the early MEG studies to provide early evidence of coherence between muscle and contralateral MI. A more recent study specifically examined CMC within the gamma (>60 Hz) frequency band, using MEG and EMG (Muthukumaraswamy, 2011) while participants performed 3 different motor tasks. The first task required simple abduction of the index finger, the second task required repetitive abduction of the same finger, and the third task required isometric contraction of the 1DI muscle against a medium (3N) or large (6N) force. The authors examined contralateral M1 response to each task as well as any potential coherence between the muscle's EMG and contralateral M1. The main finding was that although all three experiments resulted in a burst of gamma band activity in the contralateral M1, the third experiment, which required greater force than the other two, did not result in a CMC pattern within the 30-50 Hz range. The first two experiments showed CMC within the 30-50 Hz rhythm as well as cortical activity in the gamma and beta frequency band, whereas the third experiment only showed a burst in gamma activity. These results again support the possibility that the gamma band is involved in motor tasks requiring a greater force, whereas tasks requiring less force produce activity in the beta band.

2.10 Current Project

The current project will use graph theory in conjunction with CCC analysis of MEG data to identify the neural network associated with a unilateral UL task in a group of non-disabled participants. Due to its combination of temporal and spatial resolution, MEG is an optimal tool for conducting FC analysis and has also proved to be a useful tool for applying graph theoretical measures to the functional data recorded (Bassett et al., 2006, Bardouille and Boe, 2012).

Despite the variation in data analysis techniques and modalities used for recording purposes, motor networks associated with UL tasks have been identified previously (Grefkes et al., 2008, Kuhtz-Buschbeck et al., 2008, Bardouille and Boe, 2012). In general, these previous studies are lacking the application of analysis techniques to quantitatively characterize the motor network. Applying graph theory to results obtained through CCC analysis has permitted the quantification of these parameters for the neural nodes of interest. As previously described, the study by Bardouille and Boe (2012) utilized FC in conjunction with graph theory to successfully quantify the sensorimotor network. However their paradigm had participants perform a bilateral UL task in the MEG environment. While a bilateral task does elucidate the network underlying motor task performance it does not allow the separation of the brain regions that interact during a unilateral task alone. Gaining insight into the unilateral network is important for future applications of this knowledge to populations with unilateral brain lesions that result in hemiparesis, such as the case of stroke. The current project will implement a unilateral task but follow closely a similar analysis paradigm.

Using state-related CCC analysis techniques, the current study will examine differences in activation between the spatial pattern of FC observed during performance of a visually cued unilateral power gripping task and the pattern of FC during rest to elucidate the neural network that is activated during motor task performance.

Hypothesis 1: It is hypothesized that there will be a significantly different pattern of FC during the task than during rest.

Hypothesis 2: Furthermore, FC will increase predominantly between nodes of the sensorimotor network that are contralateral to the movement. Specifically, increased connectivity is expected between nodes in the contralateral M1, PMCv and PMCd

respectively as well as the ipsilateral CB, and the SMA. Also, since it is a visuomotor task, increased connectivity is also expected between V1 and regions of the sensorimotor network.

Hypothesis 3: A task-related increase in FC will result in an increased node degree for regions in the task-positive network, indicating their importance within the network. In relation to graph theory, it is hypothesized that the SMA will have the highest node degree, proving itself to be a hub between separate neural areas involved in a visuomotor task. This is based on the previously discussed findings of the significant activation of the SMA in a myriad of motor tasks.

It is also important to note that the current project is a portion of a larger study that plans to test post-stroke patients on the same paradigm used in the present study. Comparisons will be made between patients and non-disabled controls in an attempt to uncover differences in the network nodes and the nature of their configuration. The current study will determine the sensorimotor network efficiency through calculating mean path length as well as clustering coefficient. Also it will determine if the sensorimotor network is a small-world network. Determining these values will establish a baseline pattern of 'normal' network efficiency, to which patient data collected in the future will be compared. This will in turn guide future studies that use neural stimulation as a rehabilitative tool. Providing researchers with information about the importance of different neural regions in the sensorimotor network can help increase the efficiency of the rehabilitative process, resulting in greater behavioral outcomes for patients. To date, studies that used brain stimulation as a rehabilitative tool have focused on the primary motor cortex only (Grefkes et al., 2010). However, comparisons between patients and

controls may highlight novel, more functionally important areas within the sensorimotor network (e.g., having a high node degree) to be used as potential stimulation sites.

CHAPTER 3: METHODS

3.1 Participants

The study involved 21 young (20-34 years old, 25 ± 4, 12 females), healthy, right-handed participants who were free of neurological impairments as well as being both MEG and MRI compatible as determined by a pre-screening form (See Appendix A). Handedness was confirmed using the Edinburgh (Oldfield, 1971) handedness questionnaire (See Appendix B, group score = 76 ± 17). All participants were given $25 at the onset of the study to offset costs associated with study participation (e.g., parking, transportation). The study was approved by the Research Ethics Boards of the participating institutions, including the IWK Health Centre, Capital District Health Authority, and the National Research Council of Canada. Written informed consent was obtained from each individual before participation.

3.2 Task Choice

For the current project, all behavioural and neuroimaging data was acquired while the participant performed a unilateral UL task in the MEG scanner. The task was designed to elicit activation in brain regions related to motor task performance, as well as being accessible to patients post-stroke with intact ability for mass grip with the affected UL.

Being a unilateral task, it is expected (in non-disabled participants) that the majority of activation will occur in the hemisphere contralateral to the limb used for task performance, apart from the ispilateral CB. Previous research has shown that using a bilateral task causes neural activation across the entire brain, making it more difficult to localize activity produced by a specific limb (Boe and Bardouille, 2012). In patients who

have had a stroke, cerebral infarcts are almost always unilateral in nature, therefore it is important to only examine lateralized hemispheric activation in healthy controls. In the future phase of the current project, when stroke patients are scanned, the activity will not be confounded by bilateral limb activation, enabling us to infer that contralesional activation is likely caused by the compensatory changes in the brain following stroke. Another important feature of the task is that it requires a power grip (i.e., all 4 fingers, thumb and the palm), as opposed to a pinch grip or other motor task requiring a finer degree of motor control. The use of a power grip task will enable a large cohort of patients to be involved with the study in the future.

3.2.1 Task Overview

The task utilized in the current study was a custom-designed visuomotor paradigm programmed and presented using the Presentation software package (Neurobehavioral Systems, Albany, CA). The visuomotor paradigm was projected from outside the MSR through a series of mirrors onto a screen placed in front of the participant. The screen was placed one meter in front of the participant, and the projector was adjusted such that the main task screen was 27 centimetres tall to ensure a consistent, appropriate visual angle for all participants. Due to the effect eye movements have on MEG imaging data (i.e. artefacts), it was important to ensure participants could view the entire paradigm without having to move their eyes. The task required participants to use a power grip to squeeze a MEG-compatible force sensor (Current Designs, Philadelphia, PA, see Figure 4) with their non-dominant hand when prompted, to move a cursor vertically towards a moving target. The distance the ball moved was directly proportional to the force used to squeeze the sensor. The force generated by the participant was transmitted to the acquisition computer as a voltage. Once a response was made, the software determined the strength

of force of the response and generated movement of the ball on screen by converting the voltage from the device into the distance moved on screen. The harder the grip was squeezed, the greater distance the ball would travel. The target was a horizontal grey bar that moved repeatedly up and down the screen at a constant speed. The task was designed so that the target bar had an equal probability of being in any of 10 equally sized regions of the task screen. This ensured all participants would be required to use a soft, medium, and strong grip equally in order to achieve a high degree of accuracy. The maximum grip force was roughly 25% of MVC.

Figure 4: Grip Force. Grip Force (Current Designs, Philadelphia, PA) used by all participants during the task. It was held with their non-dominant (left) hand using a power grip. Once the participant made their response by squeezing the device, the voltage (power) was translated to the distance that the cursor moved on screen.

Performance-related outcomes were recorded, including *accuracy* (number of times the cursor either landed on ('hit') or did not land on ('miss') the target bar) and

error (distance between the ball and the target). The behavioural data will be subjected to analysis in a parallel study (unrelated to this thesis) to examine learning related changes and underlying brain activity. For the present study, performance data allowed us to assess participant engagement in the task, which is important to ensure all participants were focusing on the task, thereby providing a similar level of arousal across all participants.

3.2.2 Task Details

Each study session was divided into 7 blocks comprised of rest, test or training, with the test and training blocks made up of 700 trials of the visuomotor task. MEG data was collected throughout all study blocks. The first block was a 5-minute 'Rest' scan, which required the participant to sit still in the MEG scanner with their eyes closed while we recorded a baseline measurement of neural activity. The second scan block contained 50 'test' trials, wherein the ball turned invisible upon squeezing the force sensor and no feedback was given to indicate if they hit or missed the target bar. The third, fourth and fifth blocks included 200 'training' trials each, wherein the participant could see the ball move and they also received visual feedback on whether they hit or missed the target ("Great Job" or "Try Again"). The sixth block was exactly like the first task block and was considered a final test block to assess changes in performance. An additional rest block was completed as the seventh block. As well, the software (via the presentation computer) sent event markers (or *triggers*) to the MEG electronics to indicate the timing of all events in the paradigm during task performance. There were 6 types of triggers in total, "Relax", "Cue", "Go", "Move", as well as Incorrect Feedback, and Correct

Feedback.

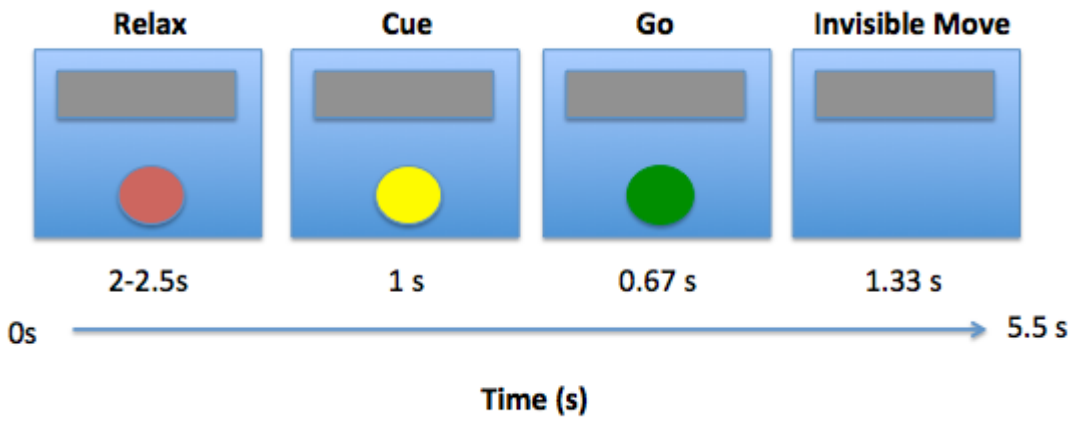

Figure 5: The timing for 1 single trial of the Test block. Each trial lasts approximately 5.5 seconds. A trial begins with the Relax phase (red cursor), followed by the Cue (yellow cursor), and finally the Go (green cursor), whereby the participant is required to make their response in less than 0.67 seconds. The cursor then disappears for the move (invisible).

Figure 5 shows the timing for a single trial of the paradigm during the test blocks. Each trial began with the 'Relax' phase, wherein the ball was red for a random interval between 2 and 2.5 seconds. The presentation of a yellow ball cued the participant that the 'Go' phase was imminent. This 'Cue' phase lasted for 1 second. The ball then turned green ('Go') and the participant had 0.67 s to make a response. Participants were instructed to make their response as quickly as possible following the 'Go' cue. If participants waited longer than the 0.67 seconds, the trial was skipped and scored as a miss. In the test blocks, the ball turned invisible when the response was made and the participants were not given feedback about performance. However, the Presentation

program still recorded the final position of the target bar and cursor (after an invisible movement). In the Training blocks, participants were able to see the ball move based on the applied force, and words appeared on screen to tell the participant whether they were correct or incorrect ("Great Job" or "Try Again" respectively).

It is important to note that the present study only analyzed data from the first rest and test blocks. All other blocks were recorded as a part of the larger study described above and will be analyzed in the future.

3.3 Choice of Response Device

Preliminary work determined the parameters for the force grip device used in the study. To do this, a group of 20 participants (23-36 years old, 27 ± 5 years, 9 females) were randomly chosen and asked to perform a maximal power grip using a handheld dynamometer (JAMAR; Sammons Preston Inc., Warrenville, IL). Each participant was asked to sit, holding the dynamometer upright in their non-dominant hand while keeping their arm at their side with their elbow at 90 degrees of flexion. Participants were given 3 trials (with a 30 second break between trials) to squeeze the dynamometer as hard as they could resulting in a maximum grip force of 368.5 ± 72.0 N (Table 1). The imaging paradigm was designed to have participants work at a submaximal level to ensure they do not experience muscle fatigue and also to ensure that in the future phase of the study, patients post-stroke can participate. Based on this requirement, a MEG-compatible force sensing device with a range of 100 N was chosen, which is roughly 25% of the maximal power grip exerted by a group of young healthy controls.

Table 1. Maximal Power Grip Results. The table provides participants' ages, gender, and the average force produced after 3 consecutive maximal grips.

Participant	Age	Gender	Average Force (N)
1	27	M	476.6
2	23	M	464.0
3	25	M	464.34
4	28	F	320.46
5	22	F	281.22
6	25	M	444.72
7	23	M	418.56
8	23	F	294.3
9	25	F	333.54
10	22	F	359.7
11	21	F	287.76
12	23	F	340.08
13	34	F	300.84
14	34	M	418.56
15	36	M	405.48
16	36	M	431.64
17	25	M	444.72
18	26	M	287.76
19	23	F	268.14
20	31	M	333.54
Average	27		368.86
Standard Deviation	5		72.06

3.4 MRI Acquisition

In order to maximize the spatial localization accuracy of MEG imaging, all participants had a structural MRI which was used in a later step whereby neural activity recorded using MEG was overlaid onto each participant's own MRI.

All participants were pre-screened before entering the MR scanner (see Appendix A for the pre-screen form). This ensured that participants did not have metal in their bodies, any psychological illness, or any other factor that would preclude their participation or influence the results of the study. Also before entering the scanner, participants were required to change into a hospital gown, to ensure their clothing did not

produce any artefacts within the magnetic field. Participants were then placed in the scanner and given a blanket.

All 3D anatomical images were collected using a 1.5T MRI scanner (GE Medical Systems, Waukesha, WI) operated by and located in the IWK Health Centre. T1-weighted images were collecting using a fast-spoiled gradient echo with inversion recovery prep sequence. The following parameters were used: field of view = 25.6 cm, slice thickness = 2mm (with a Zip2 factor resulting in a 1mm slice), frequency = 256, phase = 256, one excitation, bandwidth = 15.63 Hz, TE = Min Full, flip angle = 12°, prep time = 400 ms, number of slices = 108.

3.5 MEG Acquisition

3.5.1 Participant Preparation

When each participant entered the MEG lab, they were asked to remove any metallic objects they may have on their person. This included, but was not limited to, jewellery, phones and keys. Each participant was then shown the MEG scanner, and asked to take a seat so that an artefact check may be completed. This required the participant to be raised into the MEG helmet, and asked to remain still for roughly 30 seconds. This artefact check ensured the participants were not generating any magnetic signals that would interfere with the subsequent recordings. Provided no artefacts were discovered, the participant was asked to leave the MSR and move to the participant preparation station. In one instance a female participant generated a noticeable artefact that would negatively affect results. It was determined that she was wearing eye make-up that must have contained metal. After washing it off, another artefact check was conducted and no artefacts were subsequently discovered.

Prior to entering the MEG scanner to complete the task, a total of nine self-adhering Ag/AgCl electrodes (3 x 3 cm; Kendall-LTP, Chicopee, MA) were attached to each participant for electrophysiological recordings. To attach these electrodes, all recording sites were first prepared by abrading the skin lightly with NuPrep Skin Gel (Weaver and Company, Aurora, CO) to ensure minimal impedance followed by cleaning the area with an alcohol swab to ensure good adhesion. Electrodes were then placed above and below the left eye to record vertical electro-oculogram (VEOG), and outside the corner of each eye to record horizontal electro-oculogram (HEOG). Electrodes were also placed 2 cm apart on the anterior forearm of the non-dominant (left) arm to record muscle activity from the long flexors of the digits (e.g., flexor digitorum superficialis, flexor pollicis longus), as an electromyogram (EMG). As well, electrodes were placed on the inside of each bicep to record an electrocardiogram (ECG). Finally, a single electrode was placed on the collarbone to serve as a ground. Electrodes were affixed using Tagaderm transparent film dressings (3M, London, Ont). The EOG and ECG data were used as reference signals for the offline removal of MEG artefacts due to eye movements and cardiac activity, respectively. The EMG data enabled us to determine when the behavioral response was made.

3.5.2 Head Position Estimation

In addition to attaching electrodes to record physiological measures, each participant was set up for head position monitoring. To prepare for head position monitoring in the MEG, an electromagnetic stylus (Polhemus digitization device, Polhemus Incorporated, Vermont, USA) was used for head digitization. Three anatomical landmarks (the nasion, as well as the right and left pre-auricular points) were digitized as well as the positions of 4 head position indicator (HPI) coils. These coils were placed on

the forehead just below the hairline above each eye (x2), and one behind each ear on the mastoid process. HPI coils were also affixed using Tagaderm transparent film dressings. Finally, approximately 200 locations on the surface of the scalp were digitized with the stylus to create a 3D structure of the participant's head. The HPI coils were activated during MEG scanning, and were localized offline to monitor the participant's position within the MEG helmet. The digitization data was also used to co-register MEG data to the structural MRI (based on the 3D model), providing us with millimeter MEG source localization accuracy (Koessler et al., 2007).

After all electrode placement and digitization was completed, the participant was ready to enter the MSR to be placed in the MEG scanner. Once seated under the MEG helmet, the participant was then given one MEG compatible force grip sensor in their non-dominant (left) hand, which they used to make their behavioral response. Participants were then instructed on how to perform the task using a standardized script (Appendix C).

3.5.3 MEG Data Acquisition

All MEG data were recorded using a 306-channel whole-head Elekta Neuromag system (Elekta AB, Stockholm, SE) located within and operated by the IWK Health Centre. Data were acquired at a sampling rate of 1500 Hz, and a bandwidth of 0-500 Hz using proprietary software (Elekta AB, Stockholm, SE). Using a low-pass frequency of one third of the recording frequency ensured that we did not violate the Nyquist theorem, thus avoiding aliasing signals from 750-1500 Hz into the 0-750 Hz range (Nyquist, 1928). A low frequency (high-pass) filter setting of 0 Hz was selected to allow detection of slow wave activity including the readiness field, which is a slow change in the magnetic field associated with the preparation for a motor task (Deecke et al., 1982,

Cheyne and Weinberg, 1989). Recording at this bandpass allows for the future analysis of event-related activation, not related to the current thesis. Magnetic fields were recorded at 102 sites, with each site measuring the magnetic fields within the head on one magnetometer (in Tesla) and two planar gradiometers (in Tesla/cm^2). In addition, the MEG acquisition software also recorded VEOG, HEOG, ECG, and EMG, at a rate of 1500 Hz on the same electronics along with the triggers produced from the Presentation software. The software also continuously monitored head position via the HPI coils that were placed on each participant.

3.6 Data Analysis - Single Subject Analysis

3.6.1 Behavioral Data

As outlined previously, the presentation software recorded each participant's performance on the behavioral task. Both the location of the cursor and bar on screen were recorded and were used to calculate the error. By default these values were recorded in pixels, however they were converted to cm by multiplying them by 0.0293. Also each participant's accuracy was recorded. The EMG activity was visually inspected in relation to the cues, to determine if behavioral responses were made at the appropriate times (i.e., after the Go cue). Task compliance is indicated by appropriately responding.

3.6.2 MEG Pre-processing

Prior to statistical analyses, all MEG data were pre-processed. The first step was to *Maxfilter* the data with the Elekta Neuromag software (Elekta AB, Stockholm, SE), using the temporal signal space separation (tSSS) method. In general terms, applying tSSS to the data spatially filters it and attempts to exclude any external noise that is detected from outside of the head. The tSSS method has been shown to be a useful and efficient tool for improving the signal-to-noise ratio of MEG data (Taulu, 2009). The

second step was to create the head position estimation file, again using Elekta Neuromag software. This command utilizes the head position data recorded through the scanner (based on the HPI coils) and generates a file containing the coordinates (in mm) of each coil in space, represented in a 3-dimensional plane. Both head position estimation data sets (rest and test) for each participant were then checked using the Maxfilter program (Elekta AB, Stockholm, SE) to determine any movement during the scan. A dataset was discarded if the participant rotated more than 5 degrees, or shifted more than 5 mm in any direction. The data was then down sampled from 1500 Hz to 250 Hz and a low-pass filter of 70Hz was applied to filter out high-frequency noise. An additional artefact removal was done using a custom Matlab script (Mathworks, Natick, MA). This artefact removal utilized an independent component analysis (ICA, Hyvarinen et al., 2010). Specifically, the ICA-based analysis is an automated function that looks for linear, independent signals (components) in the data and removes any components that are assumed to be caused by external sources and not the brain. This assumption is based on temporal correlations between the components and the activity from the EOG or ECG channels.

3.6.3 MRI Pre-processing

To allow for group comparisons, MRI pre-processing registered each participant's own MRI to Talairach-Tournoux template space using the Freesurfer software package (Martinos Center for Biomedical Imaging, Massachusetts, USA). This fits each participant's brain to a common space to enable comparison of MEG source activity from the same source location between people. In addition to fitting each participant's brain to the template space, we also created a boundary around the brain, termed *boundary element model* (BEM), using Freesurfer. The use of a BEM created a refined shape of the brain boundary that was used for MEG source localization. A boundary was drawn

around the participant's brain to constrain source estimation. The BEM model is widely used in MEG- and EEG-based imaging and has been shown to be more accurate than spherical models in calculating the forward solution (Fuchs et al., 1998).

3.6.4 MEG-MRI Co-registration

In order to further increase the accuracy of the source localization, each participant's structural MRI was co-registered to match the digitized structure created during the head position estimate phase. Co-registration required two steps. The first step was to manually pinpoint the landmarks (nasion, left and right preauricular points) on the participant's MRI using the propriety MRI viewing software MRIView (Elekta AB, Stockholm, SE). Then, the 3D head image created during the digitization step was overlaid onto the structural MRI. The newly created MRIView landmarks were then adjusted so that they were within a 5mm agreement with the landmarks of the 3D head image. A quality assurance check was done by examining the location of the 200 points that were digitized prior to the MEG scan. In all cases the digital image of the head fit the anatomical MRI (i.e., the 200 points were located on the surface of the anatomical MRI). The BEM was then overlaid onto the co-registered MRI using a custom Matlab script. Using MRIView, the alignment of the BEM and MRI was checked to ensure the BEM was an accurate encapsulation of the brain that was fitted inside of the head.

3.6.5 Calculating CCC

Eighty anatomically pre-determined (Diaconescu et al., 2011, Bardouille and Boe, 2012) nodes described by their Talairach-Tournoux coordinates were used in the present study as regions of interest within the brain (for a list of nodes and their X, Y, and Z coordinates see Appendix D). These nodes were aligned to each participant's brain in 3D

space, based on the transformation defined during MRI pre-processing (MRI alignment to Talairach-Tournoux space) and MEG-MRI co-registration. Figure 6 below shows all nodes placed onto a 2D template brain for viewing perspective. It should be noted that the left and right medial premotor cortex (PMCMed) nodes were considered together as representative of the SMA due to their anatomical location. Therefore any results pertaining to the SMA are based on connections between the bilateral PMCMed nodes.

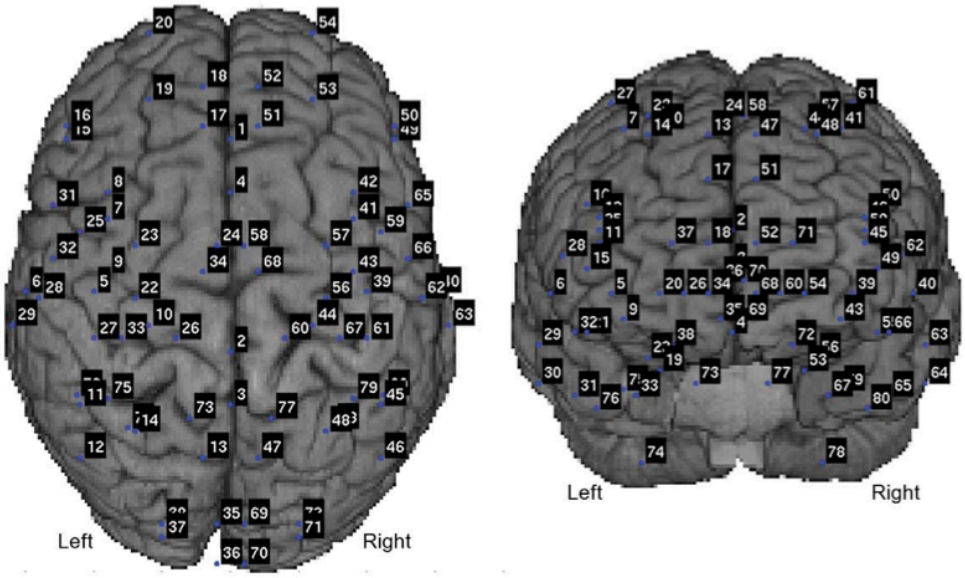

Figure 6: Anatomical Nodes used in the CCC Analysis. All 80 nodes are shown as blue dots (with their corresponding numbers) for viewing perspective on a template brain. Figure taken from Bardouille and Boe (2012).

The next step in the CCC analysis required calculating the estimated source level activity at each of the nodes across time (i.e., "virtual depth electrode") in each condition. The two conditions used were the rest block and the test (task) block. The beamformer spatial filter (Vrba et al., 2010) was used to determine activity from each node across the entire length of each scan. To calculate the source activity, the MEG data for each condition was combined with the structural MRI (containing the location of each node as

well as the BEM) to create a file containing the virtual electrode data over time at each location. Owing to variability in response time, the length of the data obtained for each virtual electrode differed. As such, all virtual electrode datasets (all test and all rest datasets) were cropped to match the shortest dataset, as calculated based on the first and last event marker. Each dataset was then epoched into durations of 250ms with a 125ms overlap for the purposes of coherence analysis. A fast Fourier transform (FFT) was then applied to each epoch to estimate the frequency content of each virtual electrode epoch at each location. The coherence between each node pair (represented as a comparison of the frequency content for a pair of virtual electrodes) was then calculated based on the FFT data to determine the amount of synchronous oscillatory activity occurring between the node pairs.

3.7 Group Level Analysis

3.7.1 Partial Least Squares Analysis

Using a custom Matlab script, a PLS analysis (McIntosh and Lobaugh, 2004) was applied to the CCC results to determine if there was a significant difference across functional connections between states (i.e., Is task different from rest?). The CCC analysis required transforming the FFT data into a 4D structure consisting of conditions (2) x subjects (19) x frequency bins (11) x node pairs (3160). During this step, only the beta band (15-30 Hz) was analyzed, therefore there were a total of 11, 1.36 Hz frequency bins. Mean-centered PLS was then applied using 512 permutations to identify latent variables (LVs) that represented a significant change in CCC across the group between conditions (rest and task) ($p < .05$) against the null hypothesis, which stated that CCC is the same between conditions. As there were only two conditions in the current study, the only LV of interest was the first LV, which indicates a change in CCC between rest and

task. A bootstrap ratio (BSR) with 512 iterations was then used to determine which frequency bins and node pairs reliably expressed this change at the 99.9th percentile. The magnitude of the BSR for each frequency bin and node-pair indicated the reliability of the conditional effect. The sign (i.e., positive or negative) of the BSR indicated if CCC for each frequency bin and node-pair increased or decreased between the two conditions. For each node pair, the maximum positive or negative BSR value was used across frequency bins. A change in CCC could have been task-positive, indicating significantly increased CCC during task compared to rest, or task-negative indicating significant decreased CCC during task as compared to rest.

3.7.2 Constructing a Task-Positive Network Matrix

Based on the results obtained from the BSR analysis on the first LV, an 80x80 coherence matrix was created. This matrix contained nodes (1-80) on both the X and Y-axis and represented all 3160 possible connections. The matrix was filtered, using the Brain Connectivity Toolbox (Rubinov and Sporns, 2010), to include only task-positive synchronous connections between nodes. This filtering first removed all task-negative connections by assigning them a value of 0 and then the remaining connections were assigned a value of 1. This process left an 80x80 binary undirected matrix representing the task-positive sensorimotor network that contained only significant task-positive connections.

3.7.3 Graph Theory Measures

All graph theory measures were calculated using the Brain Connectivity Toolbox (Rubinov and Sporns, 2010). This Toolbox is an open source Matlab package that contains the scripts necessary to perform graph theory analyses. The first measure calculated was node degree. Node degree was calculated by counting the number of

connections one node has with any other nodes, based on the binary matrix described above. According to previous literature (Bardouille and Boe, 2012), any node with a degree of three or greater is considered an important component of the network. The second measure calculated was the clustering coefficient, C. The C is calculated by determining the number of a node's neighbors (nodes that share a connection) that were also connected to each other compared to the total number of possible connections between a node's neighbors. Mean characteristic path length, L, was also calculated by averaging all shortest path lengths connecting each node-node pair.

Efficiency was calculated based on the inverse of the L. It is assumed that a more efficient network is composed of shorter path lengths between connected nodes. As this study is providing the foundation for a future study, the comparison of these graph theory metrics to the values obtained from a clinical population will provide novel information regarding changes within the diseased brain.

Finally, in order to determine if the network was a small-world network, the C and L for a random network were calculated (represented by C_{Rand} and L_{Rand}) using the Brain Connectivity Toolbox. However, to produce a more reliable measure, 20 random networks were generated in total. For each of these networks, the C_{Rand} and L_{Rand} were calculated and an average value was taken for each metric. To calculate small-worldness (S), the following equation was used where C_N and L_N represent values from the network from the present study: $S = [(C_N/C_{Rand}) / (L_N/L_{Rand})]$

3.8 Direct Links from Paradigm to Hypotheses

The first hypothesis predicts that there will be a significantly different network during task than during rest. To determine this, the PLS analysis will compare the two networks (rest vs. task), and it is expected that the first LV which states that the networks

are different, will be significant. Secondly, it is expected that FC will increase in the nodes contralateral to the active limb. Provided the task positive network is significantly different from rest, investigating the nodes that make up the task-positive network will reveal their location within the brain. Finally it is expected that the SMA will have the highest node degree. Once the FC between all regions is determined, graph theory will quantify the network based on node degree. The degree for all nodes including SMA will be tabulated to determine how many connections each node forms within the network.

CHAPTER 4: RESULTS

Out of the 21 participants scanned, 2 were removed from data analysis due to excessive head movement during the first rest scan, resulting in a total of 19 participants (11 females) aged 20-34 (25 ± 4 years) who were identified as being right handed using the Edinburgh Handedness questionnaire (76.3 ± 17.3). Unless stated otherwise, all data are presented as mean value ± standard deviation.

4.1 Behavioural Results

The target bar position was plotted for all participants across all trials, to ensure the bar had an equal probability of being in a given area across the entire task (Figure 7). The results show that the bar had a mean chance of 10 ± 1% of being in any 1 of the 10 equally sized regions.

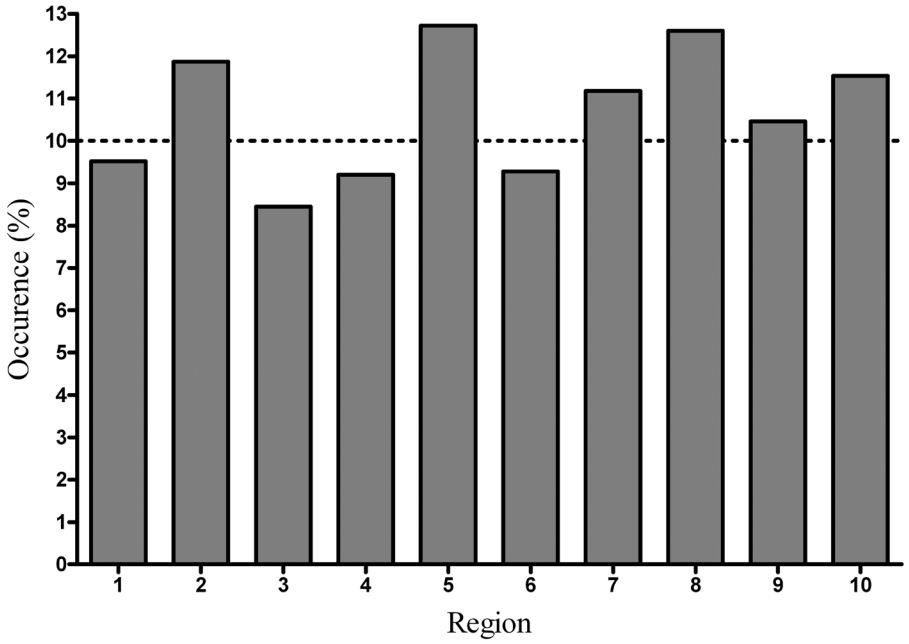

Figure 7: Location of the Bar during Test 1. The figure shows the percentage of times the bar was present in each of 10 possible locations at the time of the participants'

responses. The target was equally likely (10%) to be within any of the 10 regions during the task. The dotted line marks the 10% chance of occurrence in a given region.

4.1.1 Accuracy and Error

During the test block, participants successfully hit the target bar an average of 19.5 ± 11.25% of the time with a range of 0 (minimum) to 20 (maximum) hits (out of a possible 50). Each participant's accuracy is shown as a percentage in Figure 8. The graph indicates that performance was generally poor across the 50 trials and that there is variability between participants.

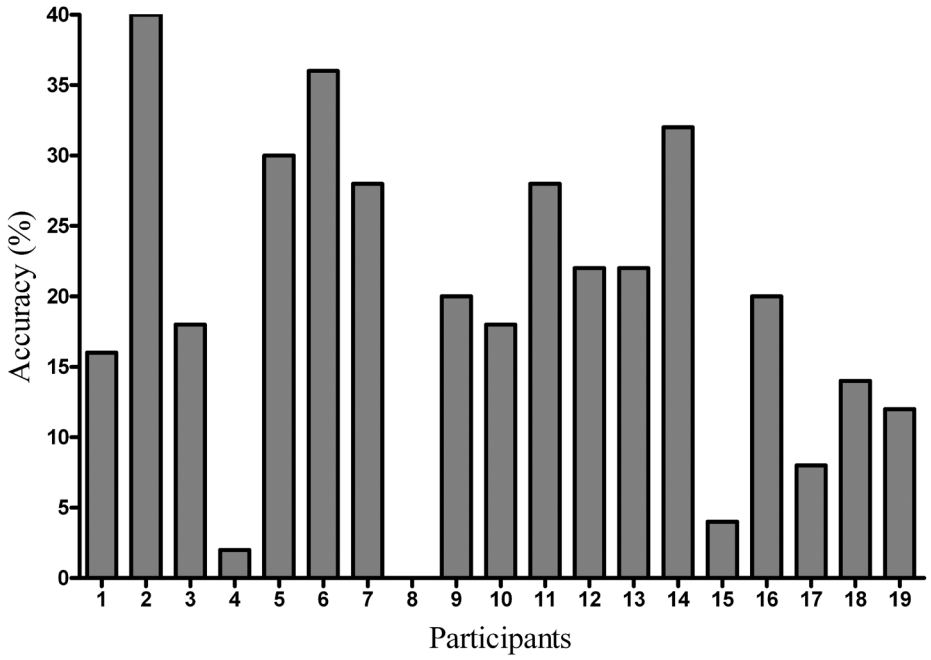

Figure 8: Accuracy During Test 1. This figure shows the percentage of times each participant correctly hit the target bar with the cursor, out of 50 possible trials. Participant 2 performed the best (40%), whereas participant 8 performed the worst (0%).

Despite poor performance during the initial test block, participants' performance improves post-training. This is illustrated by a decrease in error (Figure 9) as well as an

increase in accuracy (not shown). Figure 9 shows the error (distance between the centre of the bar and the cursor) across all 700 trials for each participant. Although learning across trials is not a component of the present study, error was examined to ensure task compliance. Participants improved throughout the task, indicating that they were performing the task properly. Also based on the visual inspection of the EMG channels, it was evident that participants were responding after the Go cue, and not during other phases of the experiment, indicating compliance with the task instructions.

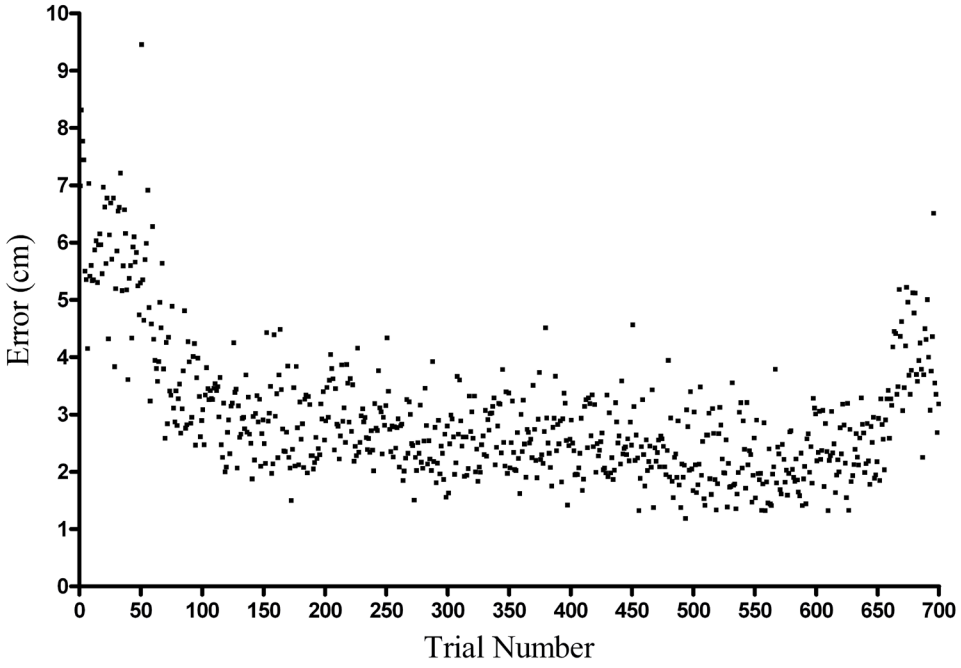

Figure 9: Error Across the Entire Experiment. The graph shows the difference (in cms) between the centre of the target bar and the centre of the cursor across all trials for all participants. It is clear from the graph that participants perform the task most poorly during the first 50 trials (Test 1), however performance improves over time.

4.2 MEG Results

Changes in CCC between node-pairs between conditions (test and rest) were identified across all participants within the beta frequency band. The first hypothesis of the present study was confirmed. The results of the PLS analysis indicate a significant difference between task and rest networks (i.e., first LV). The results of the FC analysis highlight the regions that are exhibiting increased functional connectivity during the task. The second hypothesis was also confirmed and as expected the ipsilateral CB and several regions contralateral to the moving hand, such as M1, SMA, PMC, and S1 showed increased connectivity and had high node degrees. Figure 10 below, shows the node-pairs that exhibit a reliable increase in synchrony during the task, as compared to rest (i.e., the task-positive network). See Appendix E for a list of all reliable nodes-pairs and their corresponding BSRs. For illustrative purposes, Table 2 below presents the 10 most reliable node-node pairs.

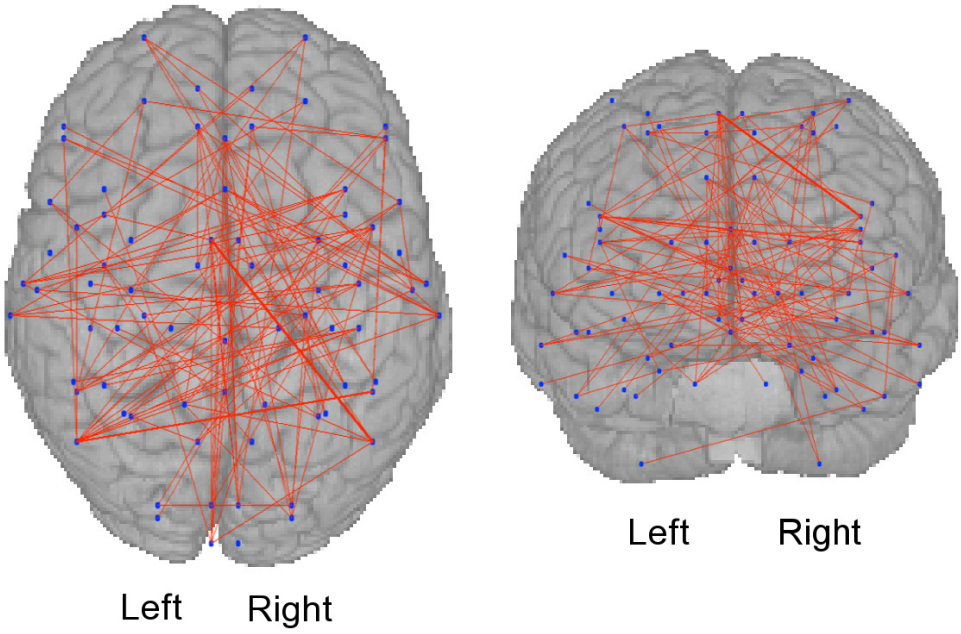

Figure 10: Beta Band Functional Connectivity between Nodes. The figure shows the task-positive network overlaid onto a template brain. Each blue dot is a node (for a total of 80) and each red line represents a connection that has increased synchrony between the two corresponding nodes during test, as compared to rest.

Table 2: Reliable Node-Pairs Determined by the BSR Analysis. Each 'Node 1' is connected to its corresponding 'Node 2', and the reliability of their connection is given. The table also provides which hemisphere the nodes are located in.

Node 1	Hemi 1	Node 2	Hemi 2	BSR
Medial Premotor Cortex	Left	Angular Gyrus	Right	8.893
Angular Gyrus	Left	Inferior Parietal Cortex	Right	6.54
Subgenual Cingulate Cortex	Midline	Middle Temporal Cortex	Right	6.211
Angular Gyrus	Right	Medial Premotor Cortex	Right	6.05
Dorsomedial Prefrontal Cortex	Left	Cuneus	Right	5.601
Primary Motor Cortex	Left	Primary Auditory Cortex	Right	5.549
Medial Premotor Cortex	Left	Primary Visual Cortex	Right	5.487
Primary Somatosensory Cortex	Right	Cruseus I	Left	5.451
Inferior Parietal Cortex	Right	Dorsolateral Prefrontal Cortex	Right	5.291
Anterior Cingulate Cortex	Midline	Fusiform Gyrus	Right	5.271

4.2.1 Task-Positive BSR Matrix

Figure 11 shows the non-thresholded BSR matrix of the task-related network as compared to rest. This matrix shows that multiple node-node pairs show increased (blue

squares) and decreased (red squares) functional connectivity during the task, as compared to rest. It is evident from the figure that both task-negative and task-positive networks are composed of multiple nodes spanning the entire brain. Figure 12 shows the binary task-positive only network matrix. Again each filled square represents a significant connection between the two corresponding nodes. Node 1 (anterior cingulate cortex) for example had one of the highest node degrees (8), which can be seen by counting the connections across the first row (or down the first column).

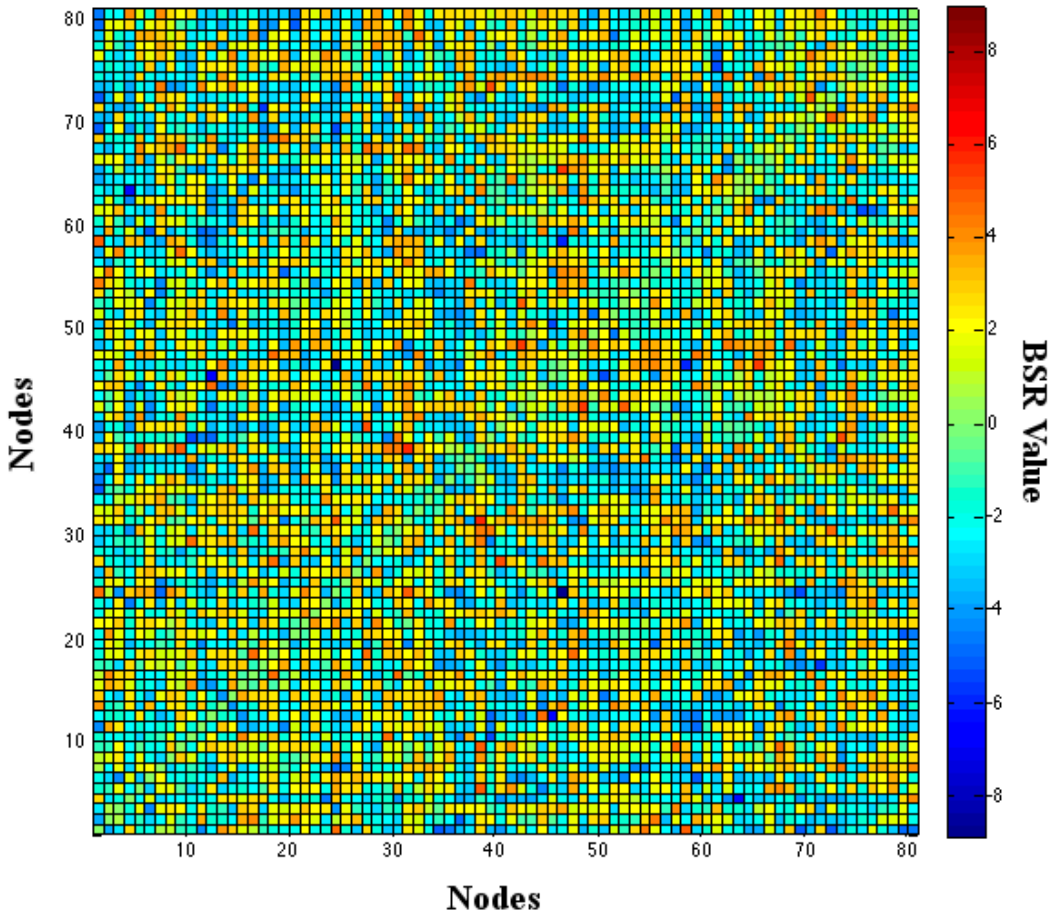

Figure 11: Non-thresholded BSR Matrix. This matrix is derived from the results of the BSR analysis. The axes represent nodes (80 total), ordered numerically. The colour in each filled square represents the reliability of the task-related change in FC between the

corresponding nodes on each axis. Cold (blue) squares represent the task-positive change in FC and all red (hot) squares are the task-negative changes in FC. The graph is mirrored along the diagonal (bottom left to top right corner).

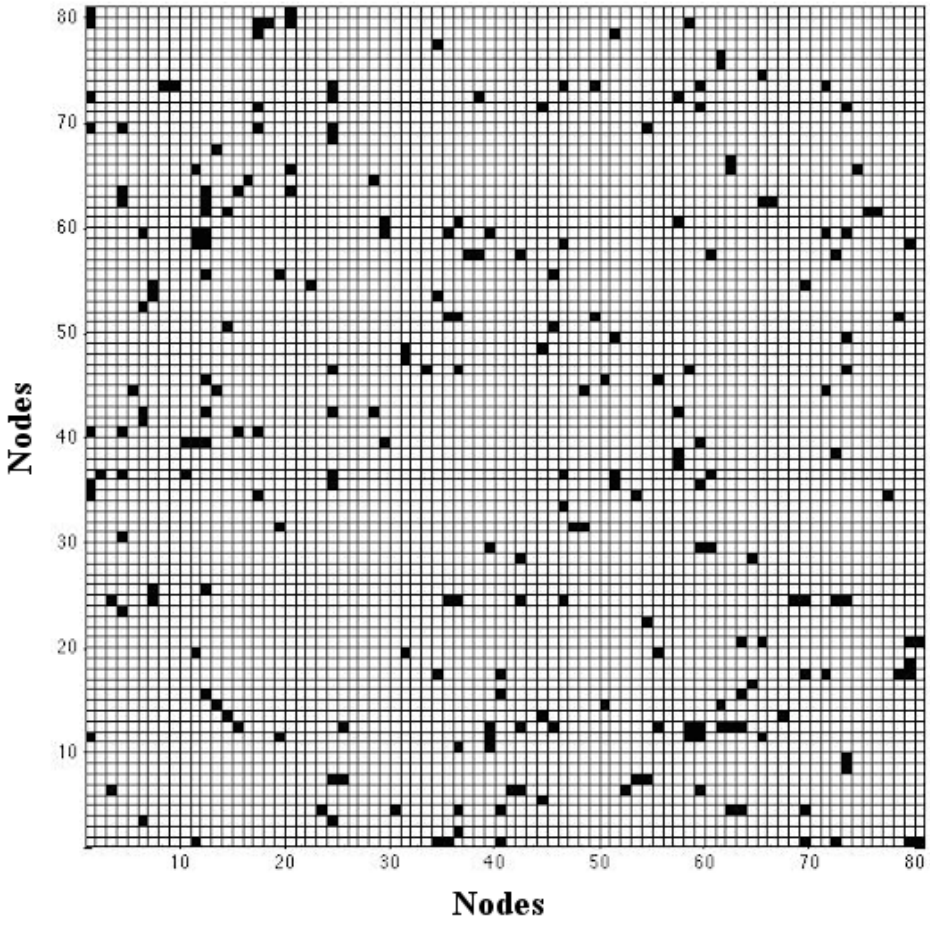

Figure 12: Binary Undirected Task-Positive Matrix. The axes represent nodes (80 total), ordered numerically. Each filled square represents a significant connection between the corresponding nodes on each axis. The graph is mirrored along the diagonal (bottom left to top right corner). Node degree may be derived from this figure by counting the connections along a column or row. For example, the top left corner square and bottom right corner square *both* represent the significant edge between the 1st and 80th nodes.

4.3 Graph Theory Measures

4.3.1 Node Degree

There were a total of 40 nodes in the task-positive network that had a degree of 3 or greater (Appendix F). Table 3 below shows several nodes with a degree greater than 3. Many of these nodes such as the SMA, PMC, the dentate (CB), M1, and S1 are considered to be relevant to the sensorimotor network as shown by previous literature (see Discussion for details concerning these regions). Furthermore the SMA (consisting of the bilateral PMCMed) had the highest node degree with a degree of 13.

Table 3. A Subset of Nodes with a High Degree. The table lists several nodes, as well as their hemisphere and degree, that are considered important within the task-positive network based on both node degree from the present study, and previous literature.

Node Name	Hemisphere	Degree
SMA	Bilateral	13
Angular Gyrus	Left	11
Anterior Cingulate Cortex	Midline	8
Ventrolateral Premotor Cortex	Right	8
Dentate	Left	7
Anterior Insula	Right	5
Dorsolateral Premotor Cortex	Right	5
Angular Gyrus	Right	5
Primary Motor Cortex	Right	4
Primary Somatosensory Cortex	Right	4
Secondary Somatosensory Cortex	Right	4

4.3.2 Other Graph Theory Metrics

The task-positive sensorimotor network found in this study had a mean characteristic path length (L) of 3.66, a clustering coefficient (C) of 0.049, and an efficiency of 0.27. The random graphs generated had an average L of 3.91, C of 0.036,

and an efficiency of 0.25. As such, the task-positive network had an S value of 1.45 indicating more small-worldness than that of a random network.

CHAPTER 5: DISCUSSION

5.1 Overview

The purpose of the present study was to highlight the task-positive sensorimotor network in a group of non-disabled controls while they performed a unilateral hand grip task. Magnetoencephalography was recorded throughout to obtain measures of brain activity while participants were at rest and during the performance of a visuomotor task. The neural networks associated with each condition were established by using FC analysis on a subset of 80 pre-determined regions of the brain. Furthermore, graph theory was applied to the network (composed of significant connections) to quantify the connections resulting from the performance a unilateral UL task.

The results from the PLS analysis revealed a significant difference in FC between the rest and task condition. More specifically, there were multiple (118) connections between node pairs present during the task condition that demonstrated increased synchrony as compared to the rest condition, highlighting a task-positive network, confirming the first hypothesis. Also graph theory has identified 40 nodes that have multiple connections with other nodes in the network, suggesting them to be key components within the network that subserves the performance of an UL, unilateral visuomotor task in non-disabled participants. As hypothesized, five of the nodes that comprise this task positive sensorimotor network represent brain regions previously established as important components of the network that underlies motor performance, including M1, S1, SMA, CB, and PMC among others, which will be discussed below. Finally the SMA was found to act as a hub within the network as demonstrated by it having the highest node degree, as posited in our third hypothesis.

The present study has improved upon previous literature by highlighting the functional connections that result from motor task performance, as compared to rest. As described in the introduction, much of the FC analyses have focused on the brain during a single state, and limited research has been done to compare interactions within the brain between separate conditions or the change in interactions across conditions. By highlighting the sensorimotor network in a group of non-disabled controls, the present study has provided a template of neural activity depicting the communication between separate brain regions, as well as a quantitative list highlighting the number of connections each region has with other regions.

As previously described, one study (Boe and Bardouille, 2012) has established and compared the functional connections within the brain between a rest and a motor task condition, however the task used was bilateral, making it difficult to infer activity from a single hemisphere. The ability to determine functional connections within a single hemisphere has many applications to clinical populations who have had unilateral brain damage. The results from the present study will be used in future studies as a baseline of activity to compare against the network of an impaired clinical population.

5.2 Evidence for Task Compliance

When performing neuroimaging research it is important to devise a paradigm that will directly enable the researcher to answer the scientific question posed. Therefore, for the present study it was important to create a motor task that was moderately difficult, required a unilateral response, was accessible to stroke patients, and required constant attention from the participants. It would have been easy to utilize a paradigm that required the participants to move their hand in the absence of any challenge or visual aid. Such a simple task should, of course, activate the motor network. However, enabling the

participants' minds to wander while they perform a simple movement is not an ideal paradigm to use for study of the motor network. By ensuring all participants were engaged in the same task, activity could be directly compared across participants as it was assumed all individual networks are representative of the task performed. As discussed in the introduction, while participants are at rest and not performing a task (i.e., 'idling'), the DMN is active, which consists of activity within different frequency bands from regions not necessarily involved with the sensorimotor network. The paradigm that was developed for the present study required concentration and skill to successfully complete. Using a challenging task ensured that all participants were focused and engaged, while enabling the passive collection of neural activation resulting from the unilateral UL movement.

Although the present study only analyzed the neural activation resulting from the first test block, examining the data across the entire experiment (all 7 blocks) provided evidence that the participants were complying with the task. The fact that error decreased and accuracy increased throughout the experiment proved that participants were focused and attempting to successfully complete the task. Furthermore, although some participants' performance was very poor (i.e. 0% accuracy) based on the EMG data it was concluded they were responding at the correct time and therefore attempting to successfully complete the task. Finally, as the MEG data indicate, synchronous beta rhythm activity between nodes of the sensorimotor network increased during the task performance block, highlighting the task's success to activate the intended network.

5.3 The Established Sensorimotor Network

The present study has demonstrated that there is a significant increase in synchrony while performing a motor task compared to resting. As expected, the observed

functional network is composed of connections between multiple regions within the brain, including areas within the contralateral hemisphere as well as the ispilateral CB. Multiple regions within this network contained a high node degree indicating their importance within the network. These nodes can be seen in Table 1 above. By examining the binary undirected matrix (Figure 12), one can determine how important a given node is by counting its connections (filled squares) across its row or column. Several of the regions (including M1, the PMC, S1, the SMA, and the CB) that had a high node degree have previously been shown to be involved in early motor learning and will be described in detail below (for a review see (Hardwick et al., 2013). Several studies, using MEG (Pollok et al., 2003) and fMRI (Floyer-Lea and Matthews, 2004, Boe et al., 2012) have shown that during a motor task, these regions are activated. However when analyzing spatial data, only inferences regarding underlying connections can be made. Through the use of FC analysis, the present study has directly shown synchrony between distinct regions, providing stronger evidence for neuronal communication. Concordance with the spatial activation patterns from earlier research increases the confidence that the functional connections found in the present study are real and related to the sensorimotor network.

5.4 Functional Connectivity

The current study used a coherence-based functional connectivity analysis and found anatomically distinct brain regions that had significantly different synchrony during a motor task, as compared to rest. This FC analysis allowed for the creation of a sensorimotor network map (Figure 10) that represents the coherence between separate regions during an active state compared to a resting state.

The present study provides novel results that show the functional connections within the brain in a group of non-disabled participants during a unilateral motor task. These results are complementary to those found by Bardouille and Boe (2012). Their study used the same analysis procedures, and highlighted the network while participants performed a very similar albeit bilateral motor task. As their results indicate, the performance of a bilateral task results in functional connections and high node degrees in multiple regions within the brain, across multiple frequency bands. As discussed in the Introduction, the literature has shown that compared to a unilateral task, a bilateral movement task results in significantly different patterns of activity across the brain as well as increased activation in areas such as the SMA. It is believed that these differences in activity manifest themselves as mechanisms to integrate and control coordination and sequential activation between the active limbs. Therefore the results of the Bardouille and Boe study can be used as a comparator for network analyses requiring a bilateral grip task, however the data cannot be segregated into separate unilateral conditions. Compared to the present study their results show that there is a higher node degree in the left PMCv within the beta frequency range during bilateral, as compared to unilateral, movement. This is likely the case because the premotor cortex is more involved in integrating information between the active limbs during a bilateral movement task. Bardouille and Boe also examined synchrony in the beta as well as the gamma (32-64 Hz) frequency range. However they found high node degrees in similar areas such as the SMA, M1, S1, and CB across both frequency bands. Both studies can now be used as templates in future FC research that uses unilateral or bilateral upper-limb tasks to determine communication within the brain.

5.4.1 Advantages to the FC Analysis Used

The use of the state-related approach in the present study is an improvement upon previous FC research. The present study sought to determine the network during a motor task. Therefore, in order to locate the regions directly related to the task, it was important to compare the task-related network against a resting state. Previous FC research has examined neuronal synchrony during rest or during a task. However, the entire brain is a network that is constantly active, even during rest, as evidenced by studies showing activation in the DMN and other networks during the resting state (Greicius et al., 2003). Therefore when examining neural activity during a single state, without comparing it to a baseline, there is the possibility of seeing activation in other networks that are also active. The state-related approach used in the present study ensures that the connections observed are a direct result of the task and are significantly different from resting state.

Another advantage to the present study methodology was that it used predefined ROIs. By determining coherence between these pre-defined ROIs, all possible connections were highlighted regardless of the power at each source. Other studies (Hoechstetter et al., 2004) employ methods that first locate ROIs based on the strength of the signal at that source, and then calculate coherence between these highlighted regions. This technique faces the possibility of missing functionally relevant coherence between active regions that are below an intensity threshold and not considered strong sources. By pre-defining regions based on anatomy, one can first calculate the activity at each region regardless of signal strength and then determine synchrony between this and other regions of similar or varying signal strengths. Using this technique in the present study ensured that all possible connections between the 80 nodes were uncovered, regardless of signal strength.

The methodology of the present study also improves upon previous literature by highlighting possible connections between 80 regions across the entire brain, as opposed to only using several ROIs. By design, the present study and analysis pipeline allows connections between any brain regions to have possibly increased and decreased synchrony during the task, and may be involved in the task-positive network. Based on this design, the network was not constrained. By using 80 nodes that span the entire brain, the present study did not exclude possible connections that may not have been found in previous work. Studies by (Xu et al., 2014) and (Sun et al., 2007) for example potentially exclude connections by constraining their network to use only limited regions of interest (13 and 5, respectively). Although activation within these regions is expected as they have been previously identified as components of the motor network, it is important to expand the literature by determining the connections between other, generally unexplored regions. For example, the present study predicted and found V1 to be a component based on the task used (visuomotor), however V1 is traditionally not assumed to be a component in the sensorimotor network.

5.5 Graph Theory Metrics

Applying graph theory to the task-positive network quantified the characteristics of node connections within the network. Therefore, the present study was able to highlight important nodes by assigning values to each node, indicating a node's relevance or importance within the network based on its node degree. Graph theory was also able to determine the mean path length (L), the clustering coefficient (C), the small-worldness, and the efficiency of the network.

As hypothesized, regions involved in the early stages of motor learning did form multiple significant connections with other regions, resulting in a high node degree for

each region. The results of the graph theory analysis produced multiple significant node-node connections that correspond with the motor learning literature. However, the literature is limited because studies have not utilized a similar approach to quantifying the sensorimotor network in a group of healthy participants. One study (Xu et al., 2014) examined the differences in the neural networks produced from a motor execution task (unilateral dominant UL) and a motor imagery task, using functional connectivity fMRI (fcMRI). Both FC analysis and graph theory were applied to the imaging data to quantify each network. The authors however used a measure other than node degree to determine a node's importance within the network, called betweeness centrality. Betweeness centrality is a measure that is based on the number of shortest paths between all nodes that cross through a specified node. It is believed that if many paths cross through a given node, it is acting as a hub within the network. Using only 13 ROIs, the authors conclude that the SMA is the only hub or 'key' node within the motor execution network in their study. Finding the SMA as a hub coincides with the present study, however there is also the possibility that a node with a very high degree is not a common intersecting point for other nodes, yet it is still important. Although the study by Xu and colleagues (2014) quantified a sensorimotor network based on a unilateral UL task, they used only 13 ROIs and found that only one node is important in the network. Perhaps identifying hub nodes, and nodes with a high node degree collectively would provide additional information in highlighting key nodes within the identified network.

As reported in the results, the sensorimotor network in the present study had a C of 0.049, an efficiency of 0.27, and an L of 3.66. Also it was found to show small-world characteristics with an S value of 1.45 (Humphries and Gurney, 2008). Having a higher

clustering coefficient and a shorter path length than a random network, characterizes the sensorimotor network of the present study as exhibiting small-world architecture.

Future studies that examine clinical populations can make direct comparisons to the values obtained in the present study. For example, when a patient post-stroke performs the same unilateral task, values for efficiency can be calculated for their sensorimotor network and compared to these baseline values derived from participants without brain injury. It is expected that a patient exhibiting impairment of the UL will have a less efficient network than the non-disabled controls of the present study. Therefore a value for efficiency of less than 0.27 is expected. In addition to efficiency, the small-worldness of the network in the present study could also be compared to networks from clinical populations performing the same task. Based on previous research examining the small-worldness of clinical populations (Micheloyannis et al., 2006), it is likely that the non-disabled motor network will be more of a small-world network than the stroke patient's motor network. For example, a study by Micheloyannis et al. (2006) found that compared to a neurologically healthy participant group, a group of patients with schizophrenia exhibited less of a small-world network. It is inferred that neurological conditions result in a disordered network that does not function as efficiently as it should. Based on this, we would hypothesize that a post-stroke neural network will also be more disordered and less efficient than the standard network obtained from those without neurological injury.

A further application of the graph theoretical measures found in the present study can be used to characterize motor learning. The present study produced the network that was active during a test block compared to a rest block. Further analysis could be conducted to determine the network during the post-training block (second test block), as

compared to rest. The post-training network could then be compared to the pre-training network to determine any quantitative differences based on significant differences in FC. As the behavioral results of the present study show, the participants learned the task with increasing practice. Based on the idea of neuroplasticity (Penhune and Doyon, 2005), it is expected that accompanying this behavioral change there should also be underlying neural changes. Given this evidence, one would hypothesize that these neural changes would be characterized by different node degrees between regions of the networks involved in the different stages of motor learning, as well as a more efficient, post-training network. More specifically, the literature (Penhune and Doyon, 2005) has shown early in motor learning there is a cerebellar-cortical network, whereas post motor learning there is a shift toward a striatal-cortical network (Doyon and Benali, 2005). Therefore one would expect a decrease in FC in the cerebellar and thalamus nodes, and an increase in regions such as the M1, S1, and SMA.

The graph theoretical analysis used in the present study showed that multiple nodes had node degrees above the threshold of three, indicating their importance within the network. Although each of these nodes are likely important components of the network, the following sections will discuss the nodes hypothesized to be involved in the network, followed by discussion related to several nodes that had a high degree but were not expected to be a part of the network.

5.6 Primary Motor Cortex

Although the performance of a motor task requires the simultaneous activation of multiple brain regions, the region most widely studied within the behavioral context has been M1. Based on the large body of literature surrounding this region, it was expected that the contralateral M1 would certainly be a key component in the neural network

highlighted by the present study. The descending pathways from the cortex form the corticospinal tract, which is directly involved with voluntary movement. Roughly 40% of the corticospinal tract originates in the motor cortex (Kandel, 2000). By having participants perform a left-handed task, the activation of the right M1 was expected and it was found. Contralateral M1 formed four significant connections with various regions of the brain during the task condition, while ipsilateral M1 had a degree of less than three. This reinforces contralateral M1's importance during a motor task and additionally, based on the results of the FC analysis, provides insight into which regions M1 is communicating with during the task.

Previous literature has repeatedly shown the importance of M1 during a motor task, beginning with Penfield and Boldrey's (1937) observation that a motor response is a result of stimulating the contralateral M1. Additionally, a meta-analysis (Hardwick et al., 2013) conducted on 39 motor learning studies that consisted of a unilateral (right) handed task only, showed consistent activation of the contralateral M1 across all studies. More relevant to the current study, the experiment previously described by Kuthtz-Buschbeck et al. (2008) showed that during a unilateral power grip task, the contralateral, not the ipsilateral, M1 was significantly activated.

The results of the present study show that one of the connections for the right M1 was to the ipsilateral superior parietal cortex (SPC). The SPC has repeatedly been shown to be important in visuomotor grasping tasks (Culham and Valyear, 2006). Therefore this connection is logical, as the choice of grip aperture for grasping is simultaneous with the motor cortex's top down command to make the response. In addition to its connection with the right SPC, M1 was also connected to the left precuneus, and the right cuneus. Several studies have shown that the precuneus is involved in ball-tracking tasks, and that

damage to the precuneus results in an impairment to track a moving target. Several other studies have also shown that the precuneus is involved with visuospatial tasks, and is involved in planning as it has direct connections to the frontal lobes (for a review see (Cavanna and Trimble, 2006). Since the present task has used a visuomotor paradigm that involves the tracking of a moving target and requires a planned response, it is not surprising that the precuneus was active and also had a significant connection with the M1, which directly controls the voluntary response.

Figure 13 below shows the motor network components that are required to perform a voluntary movement. From this image, it is evident that M1 works in conjunction with the PMC, the S1, the cerebellar cortex, and several deep brain structures, among many more. In the figure, the purple lines indicate major descending projections, and the green lines indicate either feedback projections or local connections. Except for the deep brain structures, the present study found activation in each of these regions involved with movement, however M1 did not form significant connections with these areas. A possible reason for this absence in FC between M1 and these motor regions could be that they were coherent in another frequency band such as the gamma band, and not the beta band. Although the beta band is primarily concerned with movement, several studies also show activity within the gamma band during voluntary movement (Muthukumaraswamy, 2011, Bardouille and Boe, 2012). Perhaps a voluntary motor task requires activation across multiple frequency bands, which may explain the absence of other expected functional connections between regions within this network.

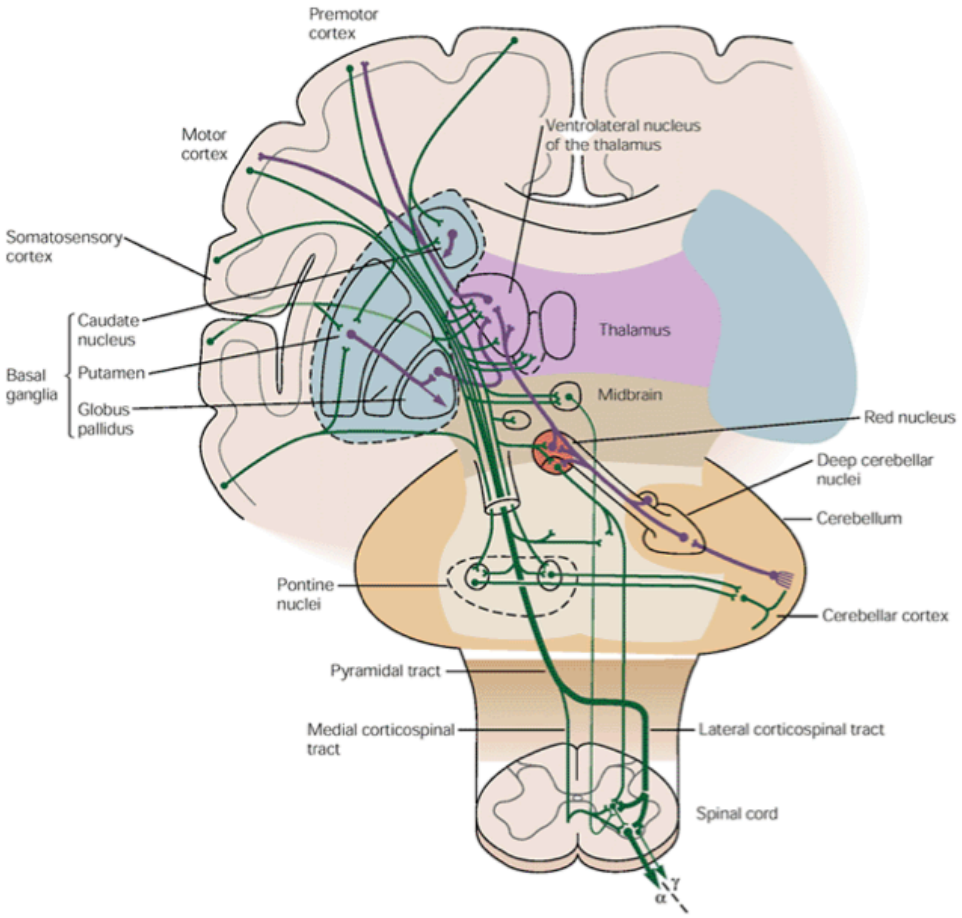

Figure 13. Brain Regions Involved with Voluntary Movement. This figure shows the regions that form the motor network responsible for voluntary movement. The purple lines are feedback projections or local connections, and the green lines are major descending pathways. The majority of the corticospinal tract (green pyramidal tract) originates in the cortex (primarily in M1) and crosses to the contralateral side of the body at the level of the medulla. Image taken from (Kandel, 2000).

5.7 Premotor Cortex

When connections from PMCd and PMCv were combined, the contralateral PMC demonstrated a node degree of 13 within the task-positive sensorimotor network in the current study. It is important to note that the PMCMed node used in the present study is

considered to represent the SMA, and will be described below. Therefore its degree was not factored into the contralateral PMC node degree calculation. Among the many connections the PMC formed with other nodes, one of these was between the right PMCv and the left inferior parietal cortex (IPC), which is expected within the context of the present paradigm. The premotor cortex has been shown on multiple occasions to be involved in motor planning and execution, especially during visuomotor tasks (for a review see (Chouinard and Paus, 2006). For example, one study examined single neuron discharge in the PMCv of the monkey and they found neural activity when the monkey grasped various objects, as well as when presented with various 3D objects (Murata et al., 1997). The IPC is considered a relay station between sensory and motor regions of the brain (Fogassi et al., 2005). The IPC has been shown to receive input from the visual stream, and as a result, patients who have lesions to his region have Optic Ataxia. This disorder is characterized by abnormal grasping when reaching for object (Sakata and Taira, 1994). Therefore one would expect a functional connection between these two regions, as both are required to perform a visuomotor task that utilizes grasping or mass grip.

5.8 *Primary Somatosensory Cortex*

In addition to the regions described above, the right S1 had a node degree of 4, indicating its importance within the network. Similar to M1, the somatosensory cortex is also topographically organized and has specific areas that are responsible for sensation on the contralateral side of the body (Kandel, 2000). Therefore, the presence of functional connections between S1 and other regions confirms our hypothesis and replicates previous literature showing that S1 is a component of the sensorimotor network.

The somatosensory cortex has repeatedly been shown to be involved in visuomotor tasks, as it is concerned with processing of somatosensory feedback. One recent study used repetitive TMS (rTMS) to assess the effects of disrupting S1 during learning a novel visuomotor task (Vidoni et al., 2010). Their study required 27 healthy right-handed participants to perform a visual tracking task by moving their wrist to move a cursor on screen. Within the experimental group, immediately before performing the task, repetitive 1Hz TMS was applied to contralateral S1 for 20 minutes. The control group received sham TMS (i.e. no pulse was delivered). The results showed that the sham TMS group had a greater reduction in tracking error for the 2 tests immediately following (sham) rTMS as well as during the retention test the following (third) day, where no rTMS was used. Therefore it is evident that S1 plays an important role in the accurate performance of a novel motor skill.

The contralateral S1 showed connections with Cruseus 1 (left), Cruseus 2 (left), SPC (left) and the angular gyrus (AG, left). Both Cruseus 1 and Cruseus 2 are regions in the CB, which has been shown to receive sensory information from the spinal cord and is directly related to ipsilateral movement (Kandel, 2000). Furthermore, both the CB and somatosensory cortex have direct connections to the thalamus, which functions as a relay station. Therefore although the CB and the somatosensory cortex do not share a direct structural connection, they are functionally connected through the thalamus.

Similar to M1, S1 was also functionally connected to the SPC. As described above, the SPC has been shown to be involved in planning and grasping actions, therefore it was expected that during a task requiring the manipulation of grasp aperture this region would be active. Furthermore, it has been shown (Sakata, 2007) that a unilateral lesion (left lateralized) to this region produces a deficit in visually guided hand

manipulation tasks, therefore activation in the left hemisphere is acceptable and it is not expected to be contralateral to the active limb.

As a final note regarding the role of S1, Bardouille and Boe (2012) also found S1 to be a part of the sensorimotor network. Although the task required bilateral movements, they found the left S1 to have a node degree of 4 during a visuomotor mass grip task, based on FC within the beta-band. From the studies outlined above, it is evident that S1 plays a major role in the sensorimotor network, especially during visuomotor tasks that require sensory feedback in order to improve task performance.

5.9 Cerebellum

As hypothesized, the ipsilateral CB was an important component of the sensorimotor network found in the present study. It formed significant functional connections with M1, S1 (as described above) and several other regions. Although not all of the eight nodes within the CB had a high node degree, one region (the dentate) did have a degree of seven, which was the 4th highest degree in the task-positive network. Previous literature has established the CB's role in motor learning and it is considered to be crucial in error detection and correction during sensorimotor tasks. An early study that confirmed this role, utilized functional neuroimaging in human participants while they performed novel sensorimotor tasks (Flament et al., 1996). The tasks required participants to use a joystick to move a cursor toward a target during standard, reverse (the cursor's movements were opposite to the joystick's), or random (the cursor's direction based on joystick movement changed from trial to trial) conditions. Participants could see their performance in real time and were provided feedback. Using these three conditions in conjunction with fMRI, the researchers found that that the CB was significantly more activated during the random condition as well as during the early stage

of learning, as compared to the standard condition. As participants' performance improved during the reverse task, cerebellar activity significantly declined. These results highlight the role of the CB in early motor learning.

A more recent study by (Galea et al., 2011) applied transcranial direct current stimulation (tDCS) to the ipsilateral CB and contralateral M1 to participants in an attempt to uncover the functional roles of these regions during an adaptive visuomotor task. The authors note that previous research using tDCS has shown its ability to increase excitability in both the CB and M1. Participants were required to move a digital stylus across a tablet, in a straight line to hit a cursor located 10 mm away. However during certain blocks when tDCS was applied to either ipsilateral CB or contralateral M1, the target was unexpectedly shifted off centre by 30 degrees. The authors found that during normal trials there were no significant differences between groups. However, during the shifted trials, the tDCS CB group showed a decrease in error. The authors inferred that anodal cerebellar tDCS enhanced task behavior. This indicates the role of the CB in adapting to and learning a changing motor task.

The present study used a unilateral grip task that required participants to vary the amount of force used, based on the moving target on screen. Similar to the studies mentioned above, early in the learning phase participants had to adjust their responses accordingly to a changing stimulus. Although the stimulus never changed unexpectedly, each trial was different and the target had to be hit at different heights on the screen. Also without receiving any feedback during this test block, it can be considered an early phase of motor learning. As such the increased FC between the CB and other regions was expected as the task required the active adaptation in movements during the early stages of a novel motor paradigm.

5.10 Supplementary Motor Area

As described in the introduction, the SMA has been studied extensively for several decades in both monkeys and humans, and has been shown repeatedly to be involved in several aspects of motor functioning. The SMA forms direct structural connections with multiple brain regions as well as with the corticospinal tract and motor neurons (for a complete overview of the SMA see (Nachev et al., 2008), providing a direct link to movement, much like M1. Based on this previous knowledge it was expected that the SMA would act as a hub and have the highest node degree, which it did.

For the present study, the SMA was considered to be composed of both the left and right PMCMed. The location of these two nodes fit into the anatomically defined region of the SMA. Before these regions were combined, the connections with each node were examined to ensure that no connection was counted twice. This occurred once whereby the right and left PMCMed both had a connection with the right AG. Therefore this connection was only counted once, leaving a total node degree of 13 for the SMA, which was the highest node degree found, proving it to be a hub within the established sensorimotor network.

An alternative approach to determining node degree for the SMA could have been done by altering the node locations prior to the analysis. A single node representing the SMA as a whole could have been defined. However the SMA is located on the midline and extends into both hemispheres. Therefore perhaps two sources would be more representative of SMA connectivity, especially based on the finding that apart from sharing one connection, both nodes made independent connections. These connections were with visual areas (V1, V2, FEF), bilateral CB, bilateral angular gyri, and left IPC among several more. As the SMA is involved with a myriad of functions such as

planning, initiating, and directing movement, as well as motor learning, connections from SMA to multiple widespread regions were expected. Since the task required vision to plan the movement, connections with the visual areas were certainly expected. Furthermore, similar to the SPC, the IPC is also involved in grasping movements, so the planning and executing of a mass grip task should consist of interaction between this region and the SMA. Finally the AG has been shown to be involved with consciousness or awareness of action as well as action discrepancy (Farrer et al., 2008). Farrer et al. (2008) conducted an experiment whereby participants performed a unilateral UL motor task and received delayed feedback. This delay between action and consequence resulted in significant activation of the right and left AG. The task used in the present study also introduced a level of discrepancy between action and consequence because the cursor disappeared once a behavioral response was made and the participants did not receive feedback. Although they were conscious of their behavioral response, they could only estimate the outcome based on how hard they squeezed the force grip device. Therefore activation in the AG is expected within the context of the present study.

5.11 Primary Visual Cortex

Finally, as expected, V1 was also an important node within the established network. Both the right and left primary visual cortices were important regions, having node degrees of five and four respectively. The analysis used in the present study required comparing a visuomotor task condition to a resting, eyes-closed condition, therefore it was expected that there would be an increase in coherence between V1 and other regions. A study by (Pool et al., 2013) examined FC using fMRI within a group of healthy participants while they performed repetitive fist closures (unilaterally and bilaterally) cued by a visual stimulus. The unilateral condition was associated with

enhanced BOLD activity within the right and left V1. Although they found activity within the V1, they however were only focused on connectivity between regions of the motor network and therefore did not provide results relating to the functional connections of V1. A study by (Culham et al., 2003) also showed visual cortex activation during a visuomotor grasping task. As stated in the previous discussion point, V1 made functional connections with the SMA, as well as the anterior cingulate cortex, bilateral prefrontal cortex, and right PMC. One study (Classen et al., 1998) used EEG to examine FC between the visual and motor regions of the brain. Using the 10-20 electrode coordinate system connectivity was examined between electrodes C3 and FC3 (representing the primary motor, sensorimotor, and premotor cortices, as well as the SMA) and electrodes O1 and O2 (representing the occipital cortices). The authors found that during a unilateral visuomotor task requiring an alternating finger pressure to trace a visually presented sinusoidal wave, there was increased beta band coherence between the motor and occipital regions, compared to a task that required the visual or motor aspect separately. The author's note that they cannot infer from exactly which region the strongest source of activity is emanating. However, it is evident that there are functional connections between the primary visual regions and those regions considered to be components within the sensorimotor network. This is in line with the findings from the current study.

5.12 Other Regions Showing High Node Degree

Apart from the regions listed above that were hypothesized to be components of the sensorimotor network, several other regions not expected to be a part of the network showed a high node degree as well (see Appendix F). These regions include the AG, and the cingulate cortex (subgenual and anterior regions).

The AG has been extensively studied using a variety of paradigms that have uncovered its multiple functions. It is involved in word processing, learning, creativity, memory, attention, and spatial cognition (for a review see (Seghier, 2013). Futhermore, the AG is structurally connected with Brodmann area 7 (Makris et al., 2007), which contains the precuneus and the SPC. Both of these regions are considered to be involved in, or functionally connected to the sensorimotor network (precuneus: Margulies et al., 2009, SPC: Sakata and Taira, 1994). Although the present study did not find any functional connections between the AG and these specific regions, the AG was found to be functionally connected to the IPC, the premotor cortex, the SMA, and the somatosensory cortices, in addition to other regions. The AG was not hypothesized to have a high node degree, however the results show that it does share several connections with important components of the sensorimotor network, which in turn are functionally connected with each other. Based on these connections it is evident that the AG was a component in the task-positive network, however this finding was unexpected and somewhat inexplicable. Perhaps it played a role as a hub between the other, important sensorimotor regions, however this role has not been established in the literature.

The cingulate cortex (CC) was not hypothesized to have a high degree in the present study, yet the subgenual and anterior regions combined had a node degree of 15. (Picard and Strick, 2001) conducted a meta-analysis on the premotor regions, and have proposed two motor components of the CC, a rostral cingulate zone (RCZ) and a caudal cingulate zone (CCZ). The CCZ is believed to be activated during movement execution while the RCZ is involved with conflict monitoring and attention/selection for action. Another meta-analysis (Beckmann et al., 2009) has found that the CC has repeatedly been involved in an error detection network (16 studies found), as well as with motor function

(23 studies found). The task used in the present study was, of course, a motor task requiring the estimation of behavioral error to perform as accurately as possible. Therefore activation of the CC, in hindsight, was reasonable.

5.13 Limitations of the present study

The present study has provided novel information to the field of MEG imaging as well as to the understanding of brain regions responsible for motor performance by using FC and graph theory to characterize the sensorimotor network in a group of non-disabled participants. The study has provided a template of FC that shows the neural activity when a group of non-disabled participants perform a unilateral UL task. However, throughout data recording and analysis there are several assumptions to be made as well as limitations to the techniques used.

The first point of discussion concerns the task performance by the participants. During the first test block, performance across all participants was poor. The most skilled participant only obtained a correct hit response of 40%, proving the task to be rather difficult initially. Poor behavioral performance however was expected, because the task used was a part of a larger study, which required participants to learn over time. Also the task did not provide feedback, so participants could not judge their performance. However, the results show that many brain regions active during this initial phase are involved in early motor learning, and support task compliance. Additionally, the poor initial performance of participants in the present study was similar to a study by Boe and colleagues (2012) that assessed changes in neural activity based on motor learning across a single session. The paradigm used was similar to the study by Bardouille and Boe (2012) and also required a bilateral UL mass grip response to move a cursor toward a stationary target. The results show that during the first 20 pre-training test trials

participants had an average accuracy of 8%, which was significantly different than the post-training accuracy, indicating that they learned with repeated training. Another study (Floyer-Lea and Matthews, 2004) examined neural activity across a single session of learning. Participants of this study performed a unilateral tracking task by squeezing a pressure sensor to move a vertical bar on screen to match another vertical bar (target pressure bar). The results showed that participants significantly improved tracking performance, which was indicated by a difference in tracking error between the first block and the last (10^{th}) block. Based on the results of these studies in addition to the present, it is not uncommon to see poor performance during the initial trials of a novel motor task. More importantly these results highlight the principle that poor performance is not a result of non-compliance.

Another limitation in the current study relates to the use of MEG for source estimation. During data analysis we are attempting to localize sources of brain activity from activity recorded outside the brain. As discussed previously, this forms the *inverse problem*, which does not have a unique solution. There are however several ways to ensure that localization is as accurate as possible. To calculate source activity from each node in the present study the virtual electrode data was calculated based on the beamformer spatial filter, using a realistic BEM for calculation of the forward solution (as described in the Methods). It is accepted that these analyses techniques provide accurate spatial localization in motor tasks (Bardouille and Boe, 2012, Cheyne, 2013). The beamformer spatial filter is a widely used method for determining activity from a specific source by attenuating all other sources of activity within the brain, and for calculating CCC across the brain. Due to its sensitivity, the beamformer is also able to detect and locate deep brain sources, which is contrary to the traditional view that MEG

is insensitive to deep brain sources. One study (Mills et al., 2012) localized activity to the hippocampus using a beamformer spatial filter, despite the hippocampus being considered a deep brain structure. During source estimation, one way to increase the accuracy is by using the actual participants' structural MRIs. The use of a participant's structural MRI ensures that all neural activity recorded is being overlaid onto the person's own brain, and not a template brain. This step also requires the successful digitization of the participant's head before the scanning occurs. By utilizing a digital head position estimation and movement tracking system, the participant's head position was monitored throughout the task with accuracy on the millimeter scale. The limitation with MEG is that unlike EEG, the sensors are stationary and when a participant moves their head inside the sensor array, source activity becomes less accurate. Therefore if a participant moves excessively, data may be lost. However based on the data obtained from the movement tracking system, any scans that contained excessive movement were removed from the analysis, ensuring the neural activity could be localized as accurately as possible. A potential issue may arise if the heads were not digitized properly, however methodological precautions were taken to ensure optimal digitization. Based on these widely used analysis procedures we can infer a degree of confidence that the location and activity of the estimated sources are accurate localizations of the real sources of neural activity.

Another potential issue with MEG imaging during the present study was that activity from all nodes may not have been independent. All neural activity studied was from 80 pre-determined nodes located across brain. The location of these nodes were based on Talairach-Tournoux coordinates, which were fitted to each participant's own MRI to ensure optimal spatial localization. The problem however arises when nodes are

close together. Magnetoencephalography sensors may not be able to distinguish between nodes that are in close proximity on the cortical surface. Therefore the activity recorded from two such nodes may be contributing to the same sensor signal, which is termed "cross-talk" between the signals (Brookes et al., 2011). This cross-talk can lead to estimates of cortical coherence that are higher than the true coherence. The present study however, examines the difference in FC between states and does not specifically focus on the absolute level of FC during each state. Since the analysis required a relative comparison between states and the location of the nodes did not differ between states, if there was cross-talk between signals, it should be consistent across scans and not affect the results.

Although the methodology of the current study had several strengths, one weakness of the analysis was that the coherence measure used did not indicate directionality of communication. The current study determined synchrony between two nodes, irrespective of information flow. For the purposes of the present study however, the coherence analysis used was appropriate to answer the study objective by quantifying the task-positive network, without the requirement to investigate the temporal order of activation (an indicator of directionality). However, knowing the direction of information flow could add to the results as previous literature has indicated directionality of multiple connections within the motor network.

5.14 Future Directions

The present study has established a sensorimotor network in a group of non-disabled controls while they performed a unilateral motor task. This network can and will be used in future studies as a template to compare against the networks of clinical populations performing the same task. By applying graph theory metrics to the

neuroimaging data obtained, the network has been quantified which allows direct numerical comparisons to be made. For example, a node of interest could be directly compared between multiple networks by comparing its node degree. Furthermore the present study has also determined the efficiency of this template network. Future studies using clinical populations can directly compare the efficiency of the diseased (or altered) network to that of a non-diseased network.

In the future this standard map of activity will be compared against a group of patients who have had a stroke. Stroke is a neurological disease that usually affects one hemisphere of the brain. By restricting blood flow and subsequent oxygen and nutrient flow to a neural region, ischemic strokes effectively kill the brain region where they occur. The majority of strokes affect the motor cortex or surrounding motor regions, which result in a physical impairment for those who experience them. The present study is important in the context of stroke research because it utilized a unilateral task, which provided a brain-wide estimation of FC based on the movement of one limb. In follow-up studies planned to supersede the current study, stroke patients will perform the same task with their affected limb. Analysis of the FC patterns within the patients' brains will likely reveal irregular patterns of activity or coherence between regions as a result of the stroke. I expect that at the location of the lesion, surrounding nodes will exhibit both a decreased functional connectivity as well as a smaller node degree compared to the non-disabled network. Furthermore I would also expect a less efficient post-stroke network, provided there was impaired behavior present. Comparing the FC patterns between patients and non-disabled controls will provide insight into how communication between regions of the brain change pre- and post-stroke.

Beyond comparing FC between patients and healthy individuals, there is ongoing research into methodologies for improving post-stroke rehabilitation based on neural stimulation (such as TMS). Grefkes et. al. (2008) has shown that when stroke patients have damage to the M1 contralateral to movement, there is an increase in activity of the ipsilateral M1 that may be working as a compensatory mechanism. Therefore one would expect a node degree shift between damaged regions of the contralateral motor network to the nodes of the ipsilateral network. In addition to this finding, Grefkes and others (2010) have shown that TMS of the affected M1 improves post-stroke rehabilitation. The problem, however, is that research into using TMS for post-stroke rehabilitation to date has only focused on this one region (M1). By determining the FC pattern within the stroke brain, different regions may be highlighted as potential targets for stimulation. The results of the present study show for example that the SMA is a major component of a non-disabled network. It would be interesting to make a direct comparison between the node degrees of SMA between the standard network and the post stroke network. Such a direct comparison could possibly unveil a functional discrepancy between networks that may provide a target for neural stimulation.

CHAPTER 6: CONCLUSION

The present study is one of few to utilize FC analysis to highlight the sensorimotor network in a group of non-disabled controls using a state-related approach, and then apply graph theoretical metrics to quantify the network. As hypothesized, this study has found a significant increase in FC during an active motor task compared to an eyes-closed resting condition. This highlights the ability of the human brain to utilize different neural networks depending on the demands of the task. Furthermore, the task-positive network contained connections between areas that have been previously shown to be specific components of the sensorimotor network and involved in visuomotor tasks, which confirmed the second hypothesis of the study. These regions include, but are not limited to, the contralateral M1, S1, PMC, SMA, V1, and the ipsilateral CB. Furthermore the third hypothesis of the present study was also confirmed, wherein the SMA had the highest degree within the network, confirming this region's role as a hub in the network supporting movement performance. The application of graph theory to this network has highlighted the importance of these regions through the calculation of quantitative measures. The application of graph theory to neuroimaging data is a relatively new approach to data analysis and therefore has much left to be discovered. However, using this analysis procedure the current project has established a baseline quantification of FC during a motor task that can be used as a comparator in future studies examining clinical populations performing behavioral ULs tasks. By comparing the important regions, as quantified with node degree, between a diseased or lesioned brain with the non-disabled population, researchers using neural stimulation procedures will have novel targets to stimulate. As this study has shown for example, among the 40 nodes considered important within the network, the SMA proved to be a hub within the network by having

the highest node degree, proving it to be a potential site in neurostimulation experiments. Locating these regions that change as a result of injury may provide useful information to aid in the rehabilitation process.

REFERENCES

Achard S, Salvador R, Whitcher B, Suckling J, Bullmore E (2006) A resilient, low-frequency, small-world human brain functional network with highly connected association cortical hubs. J Neurosci 26:63-72.

Baillet S, Mosher JC, Leahy RM (2001) Electromagnetic brain mapping. Ieee Signal Proc Mag 18:14-30.

Baker SN, Olivier E, Lemon RN (1997) Coherent oscillations in monkey motor cortex and hand muscle EMG show task-dependent modulation. The Journal of physiology 501 (Pt 1):225-241.

Bardouille T, Boe S (2012) State-related changes in MEG functional connectivity reveal the task-positive sensorimotor network. PloS one 7:e48682.

Bartolomei F, Bosma I, Klein M, Baayen JC, Reijneveld JC, Postma TJ, Heimans JJ, van Dijk BW, de Munck JC, de Jongh A, Cover KS, Stam CJ (2006) Disturbed functional connectivity in brain tumour patients: evaluation by graph analysis of synchronization matrices. Clin Neurophysiol 117:2039-2049.

Bassett DS, Meyer-Lindenberg A, Achard S, Duke T, Bullmore E (2006) Adaptive reconfiguration of fractal small-world human brain functional networks. Proceedings of the National Academy of Sciences of the United States of America 103:19518-19523.

Beckmann M, Johansen-Berg H, Rushworth MF (2009) Connectivity-based parcellation of human cingulate cortex and its relation to functional specialization. J Neurosci 29:1175-1190.

Boe SG, Cassidy RJ, McIlroy WE, Graham SJ (2012) Single session motor learning demonstrated using a visuomotor task: Evidence from fMRI and behavioural analysis. Journal of neuroscience methods 209:308-319.

Bressler SL (2002b) Event-related potentials. In: The handbook of brain theory and neural networks, pp 412-415 Cambridge, Massachusetts: MIT Press.

Brookes MJ, Hale JR, Zumer JM, Stevenson CM, Francis ST, Barnes GR, Owen JP, Morris PG, Nagarajan SS (2011) Measuring functional connectivity using MEG: methodology and comparison with fcMRI. Neuroimage 56:1082-1104.

Brovelli A, Ding M, Ledberg A, Chen Y, Nakamura R, Bressler SL (2004) Beta oscillations in a large-scale sensorimotor cortical network: directional influences revealed by Granger causality. Proceedings of the National Academy of Sciences of the United States of America 101:9849-9854.

Brown P, Salenius S, Rothwell JC, Hari R (1998) Cortical correlate of the Piper rhythm in humans. Journal of neurophysiology 80:2911-2917.

Broyd SJ, Demanuele C, Debener S, Helps SK, James CJ, Sonuga-Barke EJ (2009) Default-mode brain dysfunction in mental disorders: a systematic review. Neurosci Biobehav Rev 33:279-296.

Bullmore E, Sporns O (2009) Complex brain networks: graph theoretical analysis of structural and functional systems. Nature reviews Neuroscience 10:186-198.

Carson RG (2005) Neural pathways mediating bilateral interactions between the upper limbs. Brain research Brain research reviews 49:641-662.

Cavanna AE, Trimble MR (2006) The precuneus: a review of its functional anatomy and behavioural correlates. Brain : a journal of neurology 129:564-583.

Cheyne D, Weinberg H (1989) Neuromagnetic fields accompanying unilateral finger movements: pre-movement and movement-evoked fields. Exp Brain Res 78:604-612.

Cheyne DO (2013) MEG studies of sensorimotor rhythms: a review. Experimental neurology 245:27-39.

Chouinard PA, Paus T (2006) The primary motor and premotor areas of the human cerebral cortex. The Neuroscientist : a review journal bringing neurobiology, neurology and psychiatry 12:143-152.

Classen J, Gerloff C, Honda M, Hallett M (1998) Integrative visuomotor behavior is associated with interregionally coherent oscillations in the human brain. Journal of neurophysiology 79:1567-1573.

Cohen D (1972) Magnetoencephalography: detection of the brain's electrical activity with a superconducting magnetometer. Science 175:664-666.

Cooke SF, Bliss TV (2006) Plasticity in the human central nervous system. Brain : a journal of neurology 129:1659-1673.

Culham JC, Danckert SL, DeSouza JF, Gati JS, Menon RS, Goodale MA (2003) Visually guided grasping produces fMRI activation in dorsal but not ventral stream brain areas. Exp Brain Res 153:180-189.

Culham JC, Valyear KF (2006) Human parietal cortex in action. Current opinion in neurobiology 16:205-212.

Deecke L, Weinberg H, Brickett P (1982) Magnetic fields of the human brain accompanying voluntary movement: Bereitschaftsmagnetfeld. Exp Brain Res 48:144-148.

Diaconescu AO, Alain C, McIntosh AR (2011) The co-occurrence of multisensory facilitation and cross-modal conflict in the human brain. Journal of neurophysiology 106:2896-2909.

Doyon J, Benali H (2005) Reorganization and plasticity in the adult brain during learning of motor skills. Current opinion in neurobiology 15:161-167.

Ehrsson HH, Fagergren A, Jonsson T, Westling G, Johansson RS, Forssberg H (2000) Cortical activity in precision- versus power-grip tasks: an fMRI study. Journal of neurophysiology 83:528-536.

Farmer SF, Bremner FD, Halliday DM, Rosenberg JR, Stephens JA (1993) The frequency content of common synaptic inputs to motoneurones studied during voluntary isometric contraction in man. The Journal of physiology 470:127-155.

Farrer C, Frey SH, Van Horn JD, Tunik E, Turk D, Inati S, Grafton ST (2008) The angular gyrus computes action awareness representations. Cerebral cortex 18:254-261.

Feige B, Aertsen A, Kristeva-Feige R (2000) Dynamic synchronization between multiple cortical motor areas and muscle activity in phasic voluntary movements. Journal of neurophysiology 84:2622-2629.

Ferbert A, Priori A, Rothwell JC, Day BL, Colebatch JG, Marsden CD (1992) Interhemispheric inhibition of the human motor cortex. The Journal of physiology 453:525-546.

Flament D, Ellermann JM, Kim SG, Ugurbil K, Ebner TJ (1996) Functional magnetic resonance imaging of cerebellar activation during the learning of a visuomotor dissociation task. Human brain mapping 4:210-226.

Floyer-Lea A, Matthews PM (2004) Changing brain networks for visuomotor control with increased movement automaticity. Journal of neurophysiology 92:2405-2412.

Fogassi L, Ferrari PF, Gesierich B, Rozzi S, Chersi F, Rizzolatti G (2005) Parietal lobe: from action organization to intention understanding. Science 308:662-667.

Fries P (2005) A mechanism for cognitive dynamics: neuronal communication through neuronal coherence. Trends in cognitive sciences 9:474-480.

Friston KJ, Frith CD, Liddle PF, Frackowiak RS (1993) Functional connectivity: the principal-component analysis of large (PET) data sets. Journal of cerebral blood flow and metabolism : official journal of the International Society of Cerebral Blood Flow and Metabolism 13:5-14.

Fuchs M, Drenckhahn R, Wischmann HA, Wagner M (1998) An improved boundary element method for realistic volume-conductor modeling. IEEE transactions on bio-medical engineering 45:980-997.

Galea JM, Vazquez A, Pasricha N, de Xivry JJ, Celnik P (2011) Dissociating the roles of the cerebellum and motor cortex during adaptive learning: the motor cortex retains what the cerebellum learns. Cerebral cortex 21:1761-1770.

Gray CM, Konig P, Engel AK, Singer W (1989) Oscillatory responses in cat visual cortex exhibit inter-columnar synchronization which reflects global stimulus properties. Nature 338:334-337.

Gray CM, Singer W (1989) Stimulus-specific neuronal oscillations in orientation columns of cat visual cortex. Proceedings of the National Academy of Sciences of the United States of America 86:1698-1702.

Grefkes C, Eickhoff SB, Nowak DA, Dafotakis M, Fink GR (2008) Dynamic intra- and interhemispheric interactions during unilateral and bilateral hand movements assessed with fMRI and DCM. Neuroimage 41:1382-1394.

Grefkes C, Nowak DA, Wang LE, Dafotakis M, Eickhoff SB, Fink GR (2010) Modulating cortical connectivity in stroke patients by rTMS assessed with fMRI and dynamic causal modeling. Neuroimage 50:233-242.

Greicius MD, Krasnow B, Reiss AL, Menon V (2003) Functional connectivity in the resting brain: a network analysis of the default mode hypothesis. Proceedings of the National Academy of Sciences of the United States of America 100:253-258.

Gross J, Kujala J, Hamalainen M, Timmermann L, Schnitzler A, Salmelin R (2001) Dynamic imaging of coherent sources: Studying neural interactions in the human brain. Proceedings of the National Academy of Sciences of the United States of America 98:694-699.

Guye M, Bartolomei F, Ranjeva JP (2008) Imaging structural and functional connectivity: towards a unified definition of human brain organization? Current opinion in neurology 21:393-403.

Hagmann P, Kurant M, Gigandet X, Thiran P, Wedeen VJ, Meuli R, Thiran JP (2007) Mapping human whole-brain structural networks with diffusion MRI. PloS one 2:e597.

Hardwick RM, Rottschy C, Miall RC, Eickhoff SB (2013) A quantitative meta-analysis and review of motor learning in the human brain. Neuroimage 67:283-297.

Hart G (1991) Biomagnetometry: imaging the heart's magnetic field. British Heart Journal 65:61-62.

Hebb D, O., (1949) The Organization of Behavior: A Neuropsychological Theory. Florence, Kentucky: Psychology Press.

Herculano-Houzel S (2009) The human brain in numbers: a linearly scaled-up primate brain. Frontiers in human neuroscience 3:31.

Hoechstetter K, Bornfleth H, Weckesser D, Ille N, Berg P, Scherg M (2004) BESA source coherence: a new method to study cortical oscillatory coupling. Brain topography 16:233-238.

Hofman MA (2014) Evolution of the human brain: when bigger is better. Frontiers in neuroanatomy 8:15.

Honey CJ, Sporns O, Cammoun L, Gigandet X, Thiran JP, Meuli R, Hagmann P (2009) Predicting human resting-state functional connectivity from structural connectivity. Proceedings of the National Academy of Sciences of the United States of America 106:2035-2040.

Hopfield JJ (1982) Neural networks and physical systems with emergent collective computational abilities. Proceedings of the National Academy of Sciences of the United States of America 79:2554-2558.

Humphries MD, Gurney K (2008) Network 'small-world-ness': a quantitative method for determining canonical network equivalence. PloS one 3:e0002051.

Hyvarinen A, Ramkumar P, Parkkonen L, Hari R (2010) Independent component analysis of short-time Fourier transforms for spontaneous EEG/MEG analysis. Neuroimage 49:257-271.

Kandel ER, Schwartz, J.H., & Jessell, T.M. (2000) Principles of neural science. New York: McGraw-Hill.

Kappenman ES, Luck SJ (2010) The effects of electrode impedance on data quality and statistical significance in ERP recordings. Psychophysiology 47:888-904.

Kapreli E, Athanasopoulos S, Papathanasiou M, Van Hecke P, Strimpakos N, Gouliamos A, Peeters R, Sunaert S (2006) Lateralization of brain activity during lower limb joints movement. An fMRI study. Neuroimage 32:1709-1721.

Kim SG, Ashe J, Georgopoulos AP, Merkle H, Ellermann JM, Menon RS, Ogawa S, Ugurbil K (1993) Functional imaging of human motor cortex at high magnetic field. Journal of neurophysiology 69:297-302.

Koessler L, Maillard L, Benhadid A, Vignal JP, Braun M, Vespignani H (2007) Spatial localization of EEG electrodes. Neurophysiologie clinique = Clinical neurophysiology 37:97-102.

Kuhtz-Buschbeck JP, Gilster R, Wolff S, Ulmer S, Siebner H, Jansen O (2008) Brain activity is similar during precision and power gripping with light force: an fMRI study. Neuroimage 40:1469-1481.

Lamus C, Hamalainen MS, Temereanca S, Brown EN, Purdon PL (2012) A spatiotemporal dynamic distributed solution to the MEG inverse problem. Neuroimage 63:894-909.

Makris N, Papadimitriou GM, Sorg S, Kennedy DN, Caviness VS, Pandya DN (2007) The occipitofrontal fascicle in humans: a quantitative, in vivo, DT-MRI study. Neuroimage 37:1100-1111.

Margulies DS, Vincent JL, Kelly C, Lohmann G, Uddin LQ, Biswal BB, Villringer A, Castellanos FX, Milham MP, Petrides M (2009) Precuneus shares intrinsic functional architecture in humans and monkeys. Proceedings of the National Academy of Sciences of the United States of America 106:20069-20074.

McIntosh AR, Lobaugh NJ (2004) Partial least squares analysis of neuroimaging data: applications and advances. Neuroimage 23 Suppl 1:S250-263.

Micheloyannis S, Pachou E, Stam CJ, Breakspear M, Bitsios P, Vourkas M, Erimaki S, Zervakis M (2006) Small-world networks and disturbed functional connectivity in schizophrenia. Schizophrenia research 87:60-66.

Milgram S (1967) Small-World Problem. Psychol Today 1:61-67.

Mills T, Lalancette M, Moses SN, Taylor MJ, Quraan MA (2012) Techniques for detection and localization of weak hippocampal and medial frontal sources using beamformers in MEG. Brain topography 25:248-263.

Milner PM (1974) A model for visual shape recognition. Psychological review 81:521-535.

Murata A, Fadiga L, Fogassi L, Gallese V, Raos V, Rizzolatti G (1997) Object representation in the ventral premotor cortex (area F5) of the monkey. Journal of neurophysiology 78:2226-2230.

Murthy VN, Fetz EE (1992) Coherent 25- to 35-Hz oscillations in the sensorimotor cortex of awake behaving monkeys. Proceedings of the National Academy of Sciences of the United States of America 89:5670-5674.

Muthukumaraswamy SD (2011) Temporal dynamics of primary motor cortex gamma oscillation amplitude and piper corticomuscular coherence changes during motor control. Exp Brain Res 212:623-633.

Nachev P, Kennard C, Husain M (2008) Functional role of the supplementary and pre-supplementary motor areas. Nature reviews Neuroscience 9:856-869.

Nair DG, Purcott KL, Fuchs A, Steinberg F, Kelso JA (2003) Cortical and cerebellar activity of the human brain during imagined and executed unimanual and bimanual action sequences: a functional MRI study. Brain research Cognitive brain research 15:250-260.

Napier JR (1956) The prehensile movements of the human hand. The Journal of bone and joint surgery British volume 38-B:902-913.

Nunez PL, Srinivasan R, Westdorp AF, Wijesinghe RS, Tucker DM, Silberstein RB, Cadusch PJ (1997) EEG coherency. I: Statistics, reference electrode, volume conduction, Laplacians, cortical imaging, and interpretation at multiple scales. Electroencephalography and clinical neurophysiology 103:499-515.

Nyquist H (1928) Certain topics in telegraph transmission theory. Transactions of the American Institute of Electrical Engineers 47:617-644.

Ogawa S, Lee TM, Kay AR, Tank DW (1990) Brain magnetic resonance imaging with contrast dependent on blood oxygenation. Proceedings of the National Academy of Sciences of the United States of America 87:9868-9872.

Oldfield RC (1971) The assessment and analysis of handedness: the Edinburgh inventory. Neuropsychologia 9:97-113.

Orgogozo JM, Larsen B (1979) Activation of the supplementary motor area during voluntary movement in man suggests it works as a supramotor area. Science 206:847-850.

Penfield WB, E. (1937) Somatic Motor and Sensory Representation in the Cerebral Cortex of Man as Studied by Electrical Stimulation. Brain : a journal of neurology 60:389-443.

Penhune VB, Doyon J (2005) Cerebellum and M1 interaction during early learning of timed motor sequences. Neuroimage 26:801-812.

Picard N, Strick PL (2001) Imaging the premotor areas. Current opinion in neurobiology 11:663-672.

Pollok B, Muller K, Aschersleben G, Schmitz F, Schnitzler A, Prinz W (2003) Cortical activations associated with auditorily paced finger tapping. Neuroreport 14:247-250.

Pool EM, Rehme AK, Fink GR, Eickhoff SB, Grefkes C (2013) Network dynamics engaged in the modulation of motor behavior in healthy subjects. Neuroimage 82:68-76.

Rao SM, Binder JR, Bandettini PA, Hammeke TA, Yetkin FZ, Jesmanowicz A, Lisk LM, Morris GL, Mueller WM, Estkowski LD, et al. (1993) Functional magnetic resonance imaging of complex human movements. Neurology 43:2311-2318.

Roland PE, Larsen B, Lassen NA, Skinhoj E (1980) Supplementary motor area and other cortical areas in organization of voluntary movements in man. Journal of neurophysiology 43:118-136.

Rubinov M, Sporns O (2010) Complex network measures of brain connectivity: uses and interpretations. Neuroimage 52:1059-1069.

Sadato N, Yonekura Y, Waki A, Yamada H, Ishii Y (1997) Role of the supplementary motor area and the right premotor cortex in the coordination of bimanual finger movements. J Neurosci 17:9667-9674.

Sakata H, Taira M (1994) Parietal control of hand action. Current opinion in neurobiology 4:847-856.

Scannell JW, Burns GA, Hilgetag CC, O'Neil MA, Young MP (1999) The connectional organization of the cortico-thalamic system of the cat. Cerebral cortex 9:277-299.

Schoffelen JM, Oostenveld R, Fries P (2008) Imaging the human motor system's beta-band synchronization during isometric contraction. Neuroimage 41:437-447.

Seghier ML (2013) The angular gyrus: multiple functions and multiple subdivisions. The Neuroscientist : a review journal bringing neurobiology, neurology and psychiatry 19:43-61.

Shibasaki H, Sadato N, Lyshkow H, Yonekura Y, Honda M, Nagamine T, Suwazono S, Magata Y, Ikeda A, Miyazaki M, et al. (1993) Both primary motor cortex and supplementary motor area play an important role in complex finger movement. Brain : a journal of neurology 116 (Pt 6):1387-1398.

Singer W (1999) Neuronal synchrony: a versatile code for the definition of relations? Neuron 24:49-65, 111-125.

Sporns O (2011) The non-random brain: efficiency, economy, and complex dynamics. Frontiers in computational neuroscience 5:5.

Sporns O, Tononi G, Kotter R (2005) The human connectome: A structural description of the human brain. PLoS computational biology 1:e42.

Stam CJ, Reijneveld JC (2007) Graph theoretical analysis of complex networks in the brain. Nonlinear biomedical physics 1:3.

Stinear JW, Byblow WD (2002) Disinhibition in the human motor cortex is enhanced by synchronous upper limb movements. The Journal of physiology 543:307-316.

Sun FT, Miller LM, Rao AA, D'Esposito M (2007) Functional connectivity of cortical networks involved in bimanual motor sequence learning. Cerebral cortex 17:1227-1234.

Takasawa M, Oku N, Osaki Y, Kinoshita H, Imaizumi M, Yoshikawa T, Kimura Y, Kajimoto K, Sasagaki M, Kitagawa K, Hori M, Hatazawa J (2003) Cerebral and cerebellar activation in power and precision grip movements: an H2 15O positron emission tomography study. Journal of cerebral blood flow and metabolism : official journal of the International Society of Cerebral Blood Flow and Metabolism 23:1378-1382.

Vidoni ED, Acerra NE, Dao E, Meehan SK, Boyd LA (2010) Role of the primary somatosensory cortex in motor learning: An rTMS study. Neurobiology of learning and memory 93:532-539.

von der Malsburg C (1981) The Correlation Theory of Brain Function. Gottingen, Germany: Max-Planck-Institute for Biophysical Chemistry.

Vrba J, Robinson SE (2001) Signal processing in magnetoencephalography. Methods 25:249-271.

Vrba J, Taulu S, Nenonen J, Ahonen A (2010) Signal space separation beamformer. Brain topography 23:128-133.

Watts DJ, Strogatz SH (1998) Collective dynamics of 'small-world' networks. Nature 393:440-442.

White JG, Southgate E, Thomson JN, Brenner S (1986) The structure of the nervous system of the nematode Caenorhabditis elegans. Philosophical transactions of the Royal Society of London Series B, Biological sciences 314:1-340.

Xu L, Zhang H, Hui M, Long Z, Jin Z, Liu Y, Yao L (2014) Motor execution and motor imagery: a comparison of functional connectivity patterns based on graph theory. Neuroscience 261:184-194.

Young MP (1993) The organization of neural systems in the primate cerebral cortex. Proceedings Biological sciences / The Royal Society 252:13-18.

APPENDIX A: PRE-SCREENING FORM

MRI Participant Screening Form

Participant Code __ __ __ Date _____

Have you every worked as a machinist, metalworker, or in any profession or hobby grinding metal? ☐ Yes ☐ No
Have you ever had an injury to the eye involving a metallic object (e.g. metallic slivers, shavings, or foreign body)? ☐ Yes ☐ No
Have you ever been injured by a metallic object or foreign body (e.g. BB, bullet, Buckshot, shrapnel, etc.)? ☐ Yes ☐ No
Are you pregnant, experiencing a late menstrual period, or having fertility treatments? ☐ Yes ☐ No
Are you currently taking or have recently taken any medication? ☐ Yes ☐ No Please List: _____
Do you have drug allergies or have you had an allergic reaction? ☐ Yes ☐ No Please List: _____

Some of the following items may be hazardous to your safety and some can interfere with the MRI examination. Please check Yes or No for each of the following:

☐ Yes ☐ No	Cardiac pacemaker	☐ Yes ☐ No	Claustrophobia
☐ Yes ☐ No	Aneurysm clip or brain clip	☐ Yes ☐ No	IUD or diaphragm
☐ Yes ☐ No	Cochlear, otologic, or ear implant	☐ Yes ☐ No	Pessary or bladder ring
☐ Yes ☐ No	Implanted cardiac defibrillator	☐ Yes ☐ No	Medication patch ***(remove before scan)***
☐ Yes ☐ No	Neurostimulator	☐ Yes ☐ No	Body piercing(s) ***(remove before scan)***
☐ Yes ☐ No	Insulin or infusion pump	☐ Yes ☐ No	Metal fragments (eye, head, ear, skin)
☐ Yes ☐ No	Implanted drug infusion device	☐ Yes ☐ No	Facelift or other cosmetic surgery on body
☐ Yes ☐ No	Spinal or Bone fusion stimulator	☐ Yes ☐ No	Electrodes (on body, head, or brain)
☐ Yes ☐ No	Carotid artery vascular clamp	☐ Yes ☐ No	Aortic clips
☐ Yes ☐ No	Tissue expander (breast)	☐ Yes ☐ No	Venous umbrella
☐ Yes ☐ No	Prosthesis (eye/orbital spring or wire, penile, etc.)	☐ Yes ☐ No	Metal or wire mesh implants (Retainers/Braces)
☐ Yes ☐ No	Implant or device held in place by a magnet	☐ Yes ☐ No	Wire sutures or surgical staples, clips
☐ Yes ☐ No	Heart valve prosthesis	☐ Yes ☐ No	Harrington rods (spine)
☐ Yes ☐ No	Artificial limb or joint	☐ Yes ☐ No	Metal rods in bones, joint replacements
☐ Yes ☐ No	Other implants in body or head (radiation seeds)	☐ Yes ☐ No	Bone/joint pin, screw, nail, wire, plate
☐ Yes ☐ No	Internal pacing wires	☐ Yes ☐ No	Wig, toupee, or hair implants
☐ Yes ☐ No	Intravascular stents, filters, or coils	☐ Yes ☐ No	Hearing aid ***(remove before scan)***
☐ Yes ☐ No	Shunt (spinal or intraventricular)	☐ Yes ☐ No	Dentures ***(remove before scan)***
☐ Yes ☐ No	Vascular access port or catheters	☐ Yes ☐ No	Asthma or breathing disorders
☐ Yes ☐ No	Swan-Ganz or thermodilution catheter	☐ Yes ☐ No	Seizures or motion disorders
☐ Yes ☐ No	Tatoos, permanent makeup	☐ Yes ☐ No	Other implant _____

Please remove **all metallic objects** prior to your MR examination including: keys, hair pins, barrettes, jewelry, watch, safety pins, paperclips, money clip, credit cards, coins, pens, belt, metal buttons, pocket knife, cell phone, and beepers.

Form Completed By _____
Print Name

Signature of Person Completing Form _____ _____
Date

Adapted from: Rotman Research Institute Pre-Procedure Participant Screening Form, 2008

APPENDIX B: HANDEDNESS FORM

Edinburgh Handedness Inventory

Please indicate your preferences in the use of hands in the following activities *by putting a check in the appropriate column*. Where the preference is so strong that you would never try to use the other hand, unless absolutely forced to, *put 2 checks*. If in any case you are really indifferent, *put a check in both columns*.

Some of the activities listed below require the use of both hands. In these cases, the part of the task, or object, for which hand preference is wanted is indicated in parentheses.

Please try and answer all of the questions, and only leave a blank if you have no experience at all with the object or task.

	Left	Right
1. Writing	☐ ☐	☐ ☐
2. Drawing	☐ ☐	☐ ☐
3. Throwing	☐ ☐	☐ ☐
4. Scissors	☐ ☐	☐ ☐
5. Toothbrush	☐ ☐	☐ ☐
6. Knife (without fork)	☐ ☐	☐ ☐
7. Spoon	☐ ☐	☐ ☐
8. Broom (upper hand)	☐ ☐	☐ ☐
9. Striking Match (match)	☐ ☐	☐ ☐
10. Opening box (lid)	☐ ☐	☐ ☐
TOTAL(count checks in both columns)		

Difference	Cumulative TOTAL	Result

APPENDIX C: TASK INSTRUCTIONS

The task that we are asking you to do requires that you get the red ball to land on the gray bar. The movement of the ball is based on how hard you squeeze the grip force. The ball is going to change from red to yellow to green, much like a traffic light. After the ball turns green you make your response by squeezing the force grip. You might think that responding before the green cue is better, but we do not include that information so it is important that you only respond after the ball turns green. The harder you squeeze the handgrip, the higher on the screen the ball will go. The softer you squeeze the grip the less distance the ball will go. It is important to point out that you only get one response. You cannot correct the movement when the ball starts moving. Also before and after making a response you should relax your hand so you are not squeezing the grip, this will give us a good reading of when movement starts and ends.

Each trial will start with the task screen. Then the ball will turn from red to yellow to green. You have one second after the ball turns green to make your response. Again, the objective is to get the ball to touch the grey bar, which will move up and down the screen repeatedly.

The first test consists of 50 trials. During these trials you will not see the ball move, nor will you be told if you were correct or incorrect. This means that you will not know how well you are doing so you need to estimate where the ball is going.

The second block consists of 600 trials, broken up into groups of 200 with a break in between. During these trials you will see the ball move so you will know how well you are doing. In these trials you will get feedback that says if you hit or missed the target bar.

During the final test, you will do another 50 trials exactly like the first test and you will not see the ball move. These trials will tell us how well you learned the task.

The whole session will take roughly one hour. You will get a short break after the first 50 trials, then a break after every set of 200 trials. During each part it is important that you keep your head as still as possible. We will tell you when each part starts and ends, and you may move your head during the breaks. It's easiest to remain still if you rest your head against the back or the front of the helmet. Also blinking interferes with the scan but I understand that you have to blink so if you could try to blink after the feedback that would be great.

Do you have any questions?

Okay, lets get started. Remember that we can see you through the camera and will be able to hear you at all times. Let us know right away if you have any problems and we can come in and get you.

Rest Block Instructions

First we are going to do a 5-minute scan to get a baseline measure of activity. We ask that you please close your eyes, relax and try not to move during this time.

Test Block

In this first scan you will do 50 trials without feedback. Try your best to estimate where the ball is moving based on how hard you squeeze the force grip. Try to remain still during this Block.

Training Block

In this block you will do 600 trials, broken into 3 groups of 200 trials with a break in-between. Here you will see the ball move and you will get feedback. These trials are a little faster then the first block because the cursor does not remain red for as long. Try your best and remember to relax your hand in-between trials and also remain still during testing.

Final Test Block Instructions

In this last scan you will do 50 trials without feedback again (the same as the beginning). Try your best to estimate where the ball is moving based on how hard you squeeze the force grip. Try to remain still during this Block.

Rest Block Instructions

First we are going to do a 5-minute scan to get a baseline measure of activity. We ask that you please close your eyes, relax and try not to move during this time.

APPENDIX D: LIST OF 80 NODES AND COORDINATES

Node		Abbreviated Name	Hemisphere	X	Y	Z
Number	Name					
1	Anterior cingulate cortex	AntCC	MIDLINE	0	32	24
2	Posterior cingulate cortex	PosCC	MIDLINE	0	-32	24
3	Retrosplenial cingulate cortex	RsCC	MIDLINE	0	-48	12
4	Subgenual cingulate cortex	SubCC	MIDLINE	0	16	-8
5	Primary auditory cortex	A1	LEFT	-40	-14	4
6	Secondary auditory cortex	A2	LEFT	-60	-14	4
7	Frontal eye fields	FEF	LEFT	-36	8	56
8	Anterior insula	AntI	LEFT	-36	16	-4
9	Claustrum	Claus	LEFT	-36	-8	-4
10	Primary motor cortex	M1	LEFT	-24	-24	56
11	Inferior parietal cortex	IPC	LEFT	-44	-48	20
12	Angular gyrus	AG	LEFT	-44	-64	28
13	Precuneus	PreCun	LEFT	-8	-64	54
14	Superior parietal cortex	SPC	LEFT	-28	-56	54
15	Centrolateral prefrontal cortex	PFCCL	LEFT	-48	32	12
16	Dorsolateral prefrontal cortex	PFCDL	LEFT	-48	36	32
17	Dorsomedial prefrontal cortex	PFCDM	LEFT	-8	36	40
18	Medial prefrontal cortex	PFCMed	LEFT	-8	48	20
19	Orbitofrontal cortex	PFCORB	LEFT	-24	44	-20
20	Frontal polar prefrontal cortex	PFCFPol	LEFT	-24	64	4
21	Ventrolateral prefrontal cortex	PFCVL	LEFT	-48	32	-8
22	Parahippocampal cortex	ParHippC	LEFT	-28	-16	-16
23	Dorsolateral premotor cortex	PMCDL	LEFT	-28	0	60
24	Medial premotor cortex	PMCMed	LEFT	-4	0	60
25	Ventrolateral premotor cortex	PMCVL	LEFT	-44	4	24
26	Pulvinar	Pulvinar	LEFT	-16	-28	4
27	Primary somatosensory cortex	S1	LEFT	-40	-28	64
28	Secondary somatosensory cortex	S2	LEFT	-56	-16	16
29	Middle temporal cortex	TCMid	LEFT	-64	-24	-12
30	Inferior temporal cortex	TCI	LEFT	-64	-24	-24
31	Temporal pole	TempPol	LEFT	-52	12	-28
32	Superior temporal cortex	TCS	LEFT	-52	-4	-8
33	Ventral temporal cortex	TCV	LEFT	-32	-28	-28
34	Thalamus (ventral lateral nucleus)	Thal	LEFT	-8	-8	4
35	Primary visual cortex	V1	LEFT	-4	-84	-4

Node		Abbreviated Name	Hemisphere	X	Y	Z
Number	Name					
36	Secondary visual cortex	V2	LEFT	-4	-96	8
37	Cuneus	Cun	LEFT	-20	-88	20
38	Fusiform gyrus	FusiG	LEFT	-20	-84	-12
39	Primary auditory cortex	A1	RIGHT	40	-14	4
40	Secondary auditory cortex	A2	RIGHT	60	-14	4
41	Frontal eye fields	FEF	RIGHT	36	8	56
42	Anterior insula	AntI	RIGHT	36	16	-4
43	Claustrum	Claus	RIGHT	36	-8	-4
44	Primary motor cortex	M1	RIGHT	24	-24	56
45	Inferior parietal cortex	IPC	RIGHT	44	-48	20
46	Angular gyrus	AG	RIGHT	44	-64	28
47	Precuneus	PreCun	RIGHT	8	-64	54
48	Superior parietal cortex	SPC	RIGHT	28	-56	54
49	Centrolateral prefrontal cortex	PFCCL	RIGHT	48	32	12
50	Dorsolateral prefrontal cortex	PFCDL	RIGHT	48	36	32
51	Dorsomedial prefrontal cortex	PFCDM	RIGHT	8	36	40
52	Medial prefrontal cortex	PFCMed	RIGHT	8	48	20
53	Orbitofrontal cortex	PFCORB	RIGHT	24	44	-20
54	Frontal polar	PFCFPol	RIGHT	24	64	4
55	Ventrolateral prefrontal cortex	PFCVL	RIGHT	48	32	-8
56	Parahippocampal cortex	ParHippC	RIGHT	28	-16	-16
57	Dorsolateral premotor cortex	PMCDL	RIGHT	28	0	60
58	Medial premotor cortex	PMCMed	RIGHT	4	0	60
59	Ventrolateral premotor cortex	PMCVL	RIGHT	44	4	24
60	Pulvinar	Pulvinar	RIGHT	16	-28	4
61	Primary somatosensory cortex	S1	RIGHT	40	-28	64
62	Secondary somatosensory cortex	S2	RIGHT	56	-16	16
63	Middle temporal cortex	TCMid	RIGHT	64	-24	-12
64	Inferior temporal cortex	TCI	RIGHT	64	-24	-24
65	Temporal pole	TempPol	RIGHT	52	12	-28
66	Superior temporal cortex	TCS	RIGHT	52	-4	-8
67	Ventral temporal cortex	TCV	RIGHT	32	-28	-28
68	Thalamus (ventral lateral nucleus)	Thal	RIGHT	8	-8	4
69	Primary visual cortex	V1	RIGHT	4	-84	-4
70	Secondary visual cortex	V2	RIGHT	4	-96	8
71	Cuneus	Cun	RIGHT	20	-88	20
72	Fusiform gyrus	FusiG	RIGHT	20	-84	-12

Node		Abbreviated Name	Hemisphere	X	Y	Z
Number	**Name**					
73	Dentate Nucleus	Dentate	LEFT	-12	-52	-24
74	Posterior Lobe	PostLobe	LEFT	-30	-55	-49
75	Cruseus 1	CrusI	LEFT	-36	-46	-26
76	Cruseus 2	CrusII	LEFT	-45	-45	-32
77	Dentate Nucleus	Dentate	RIGHT	12	-52	-24
78	Posterior Lobe	PostLobe	RIGHT	30	-55	-49
79	Cruseus 1	CrusI	RIGHT	36	-46	-26
80	Cruseus 2	CrusII	RIGHT	45	-45	-32

APPENDIX E: LIST OF SIGNIFICANT NODE-PAIRS

Node 1	Hemisphere 1	Node 2	Hemisphere 2	BSR
PMCMed	LEFT	AG	RIGHT	-8.893
AG	LEFT	IPC	RIGHT	-6.54
SubCC	MIDLINE	TCMid	RIGHT	-6.211
AG	RIGHT	PMCMed	RIGHT	-6.05
PFCDM	LEFT	Cun	RIGHT	-5.601
M1	LEFT	A1	RIGHT	-5.549
PMCMed	LEFT	V1	RIGHT	-5.487
S1	RIGHT	CrusI	LEFT	-5.451
IPC	RIGHT	PFCDL	RIGHT	-5.291
AntCC	MIDLINE	FusiG	RIGHT	-5.271
AntCC	MIDLINE	V1	RIGHT	-5.158
AntCC	MIDLINE	Thal	LEFT	-5.138
A2	LEFT	PMCVL	RIGHT	-5.131
PFCFPol	LEFT	CrusI	RIGHT	-5.041
S1	RIGHT	CrusII	LEFT	-5.005
FusiG	LEFT	PMCDL	RIGHT	-5.003
AntCC	MIDLINE	CrusI	RIGHT	-4.951
PFCORB	LEFT	PFCVL	RIGHT	-4.941
AG	LEFT	A1	RIGHT	-4.909
IPC	LEFT	PMCVL	RIGHT	-4.886
PMCDL	RIGHT	FusiG	RIGHT	-4.868
FEF	LEFT	PMCMed	LEFT	-4.802
PosCC	MIDLINE	V2	LEFT	-4.746
SPC	LEFT	PFCDL	RIGHT	-4.704
PFCFPol	LEFT	CrusII	RIGHT	-4.692
AntCC	MIDLINE	CrusII	RIGHT	-4.659
SubCC	MIDLINE	PMCDL	LEFT	-4.621
AG	LEFT	AntI	RIGHT	-4.583
AntCC	MIDLINE	V1	LEFT	-4.526
V2	LEFT	Pulvinar	RIGHT	-4.523
Cun	LEFT	PMCDL	RIGHT	-4.523
AG	LEFT	PMCVL	RIGHT	-4.484
PFCDM	RIGHT	PostLobe	RIGHT	-4.47
AG	RIGHT	Dentate	LEFT	-4.464
PFCCL	RIGHT	PFCDM	RIGHT	-4.462
PFCFPol	RIGHT	V1	RIGHT	-4.447
Thal	LEFT	PFCORB	RIGHT	-4.407
PreCun	LEFT	M1	RIGHT	-4.406
PFCDM	LEFT	PostLobe	RIGHT	-4.397
V2	LEFT	AG	RIGHT	-4.388
A2	LEFT	AntI	RIGHT	-4.375
PMCDL	RIGHT	Pulvinar	RIGHT	-4.368

Node 1	Hemisphere 1	Node 2	Hemisphere 2	BSR
TempPol	LEFT	SPC	RIGHT	-4.342
PMCMed	LEFT	V2	LEFT	-4.334
PFCDM	LEFT	V1	RIGHT	-4.313
PFCDL	LEFT	TCI	RIGHT	-4.305
PFCCL	RIGHT	Dentate	LEFT	-4.3
A1	LEFT	M1	RIGHT	-4.298
TCMid	LEFT	Pulvinar	RIGHT	-4.298
FEF	LEFT	PFCFPol	RIGHT	-4.292
PMCMed	LEFT	Dentate	LEFT	-4.286
AntCC	MIDLINE	IPC	LEFT	-4.282
TCMid	LEFT	A1	RIGHT	-4.268
FEF	LEFT	PFCORB	RIGHT	-4.254
V1	LEFT	PMCVL	RIGHT	-4.247
M1	LEFT	V2	LEFT	-4.245
PFCORB	LEFT	TempPol	LEFT	-4.24
PreCun	LEFT	TCV	RIGHT	-4.235
AG	LEFT	PMCMed	RIGHT	-4.233
A2	LEFT	PFCMed	RIGHT	-4.226
FEF	LEFT	PMCVL	LEFT	-4.224
IPC	LEFT	A1	RIGHT	-4.207
IPC	LEFT	PFCORB	LEFT	-4.204
V2	LEFT	PFCDM	RIGHT	-4.189
SubCC	MIDLINE	S2	RIGHT	-4.186
RsCC	MIDLINE	A2	LEFT	-4.179
Cun	RIGHT	Dentate	LEFT	-4.169
TCMid	LEFT	PMCVL	RIGHT	-4.161
SubCC	MIDLINE	A2	RIGHT	-4.154
PFCMed	LEFT	CrusI	RIGHT	-4.148
M1	RIGHT	Cun	RIGHT	-4.126
SubCC	MIDLINE	V1	RIGHT	-4.122
PreCun	LEFT	SPC	LEFT	-4.114
PMCMed	RIGHT	CrusI	RIGHT	-4.107
SPC	LEFT	S1	RIGHT	-4.107
PFCFPol	LEFT	TCMid	RIGHT	-4.106
PMCVL	RIGHT	Cun	RIGHT	-4.094
AG	LEFT	S2	RIGHT	-4.089
FusiG	LEFT	FusiG	RIGHT	-4.086
S2	LEFT	AntI	RIGHT	-4.079
PMCMed	LEFT	AntI	RIGHT	-4.069
PFCDM	LEFT	A2	RIGHT	-4.067
AntI	LEFT	Dentate	LEFT	-4.066
AG	LEFT	PFCCL	LEFT	-4.06
TempPol	RIGHT	PostLobe	LEFT	-4.044
TCV	LEFT	AG	RIGHT	-4.012

Node 1	Hemisphere 1	Node 2	Hemisphere 2	BSR
PFCDM	LEFT	CrusI	RIGHT	-4.01
IPC	LEFT	PMCMed	RIGHT	-3.972
IPC	RIGHT	PFCVL	RIGHT	-3.967
IPC	LEFT	TempPol	RIGHT	-3.965
PMCMed	LEFT	V1	LEFT	-3.965
AG	LEFT	TCMid	RIGHT	-3.96
A1	RIGHT	PMCVL	RIGHT	-3.951
S2	RIGHT	TCS	RIGHT	-3.95
PFCDM	LEFT	Thal	LEFT	-3.95
AntI	RIGHT	PMCDL	RIGHT	-3.945
AG	LEFT	PFCVL	RIGHT	-3.942
TempPol	LEFT	PreCun	RIGHT	-3.935
AntCC	MIDLINE	A2	RIGHT	-3.931
PFCFPol	LEFT	TempPol	RIGHT	-3.931
S2	RIGHT	TempPol	RIGHT	-3.926
SubCC	MIDLINE	TCI	LEFT	-3.921
AG	LEFT	S1	RIGHT	-3.908
RsCC	MIDLINE	PMCMed	LEFT	-3.905
PMCMed	LEFT	Thal	RIGHT	-3.897
PFCCL	LEFT	TCMid	RIGHT	-3.892
S2	LEFT	TCI	RIGHT	-3.89
Claus	LEFT	Dentate	LEFT	-3.888
PFCCL	LEFT	A2	RIGHT	-3.881
ParHippC	LEFT	PFCFPol	RIGHT	-3.865
AG	LEFT	PMCVL	LEFT	-3.859
SubCC	MIDLINE	V2	LEFT	-3.857
M1	RIGHT	SPC	RIGHT	-3.856
Thal	LEFT	Dentate	RIGHT	-3.854
A2	LEFT	FEF	RIGHT	-3.838
V1	LEFT	PFCDM	RIGHT	-3.835
PMCMed	LEFT	FusiG	RIGHT	-3.833
PMCVL	RIGHT	Dentate	LEFT	-3.831

APPENDIX F: LIST OF ALL NODES WITH A DEGREE OF 3 OR GREATER

Node	Hemisphere	Degree
AG	LEFT	11
PMCMed	LEFT	10
AntCC	MIDLINE	8
PMCVL	RIGHT	8
SubCC	MIDLINE	7
V2	LEFT	7
Dentate	LEFT	7
IPC	LEFT	6
PFCDM	LEFT	6
A2	LEFT	5
A1	RIGHT	5
AntI	RIGHT	5
AG	RIGHT	5
PMCDL	RIGHT	5
V1	RIGHT	5
CrusI	RIGHT	5
FEF	LEFT	4
PFCFPol	LEFT	4
Thal	LEFT	4
V1	LEFT	4
A2	RIGHT	4
M1	RIGHT	4
PFCDM	RIGHT	4
PMCMed	RIGHT	4
S1	RIGHT	4
S2	RIGHT	4
TCMid	RIGHT	4
TempPol	RIGHT	4
Cun	RIGHT	4
FusiG	RIGHT	4
PreCun	LEFT	3
SPC	LEFT	3
PFCCL	LEFT	3
PFCORB	LEFT	3
TCMid	LEFT	3

Node	Hemisphere	Degree
TempPol	LEFT	3
IPC	RIGHT	3
PFCFPol	RIGHT	3
PFCVL	RIGHT	3
Pulvinar	RIGHT	3